# A guideline for head volume conductor modeling in EEG and MEG

Johannes Vorwerk [a,*], Jae-Hyun Cho [b], Stefan Rampp [c], Hajo Hamer [c],
Thomas R. Knösche [b], Carsten H. Wolters [a]

[a] Institut für Biomagnetismus und Biosignalanalyse, Westfälische Wilhelms-Universität, Münster, Germany
[b] Max Planck Institute for Human Cognitive and Brain Sciences, Leipzig, Germany
[c] Epilepsiezentrum, Universitätsklinikum Erlangen, Erlangen, Germany

## ARTICLE INFO

## ABSTRACT

For accurate EEG/MEG source analysis it is necessary to model the head volume conductor as realistic as possible. This includes the distinction of the different conductive compartments in the human head. In this study, we investigated the influence of modeling/not modeling the conductive compartments skull spongiosa, skull compacta, cerebrospinal fluid (CSF), gray matter, and white matter and of the inclusion of white matter anisotropy on the EEG/MEG forward solution. Therefore, we created a highly realistic 6-compartment head model with white matter anisotropy and used a state-of-the-art finite element approach. Starting from a 3-compartment scenario (skin, skull, and brain), we subsequently refined our head model by distinguishing one further of the above-mentioned compartments. For each of the generated five head models, we measured the effect on the signal topography and signal magnitude both in relation to a highly resolved reference model and to the model generated in the previous refinement step. We evaluated the results of these simulations using a variety of visualization methods, allowing us to gain a general overview of effect strength, of the most important source parameters triggering these effects, and of the most affected brain regions. Thereby, starting from the 3-compartment approach, we identified the most important additional refinement steps in head volume conductor modeling. We were able to show that the inclusion of the highly conductive CSF compartment, whose conductivity value is well known, has the strongest influence on both signal topography and magnitude in both modalities. We found the effect of gray/white matter distinction to be nearly as big as that of the CSF inclusion, and for both of these steps we identified a clear pattern in the spatial distribution of effects. In comparison to these two steps, the introduction of white matter anisotropy led to a clearly weaker, but still strong, effect. Finally, the distinction between skull spongiosa and compacta caused the weakest effects in both modalities when using an optimized conductivity value for the homogenized compartment. We conclude that it is highly recommendable to include the CSF and distinguish between gray and white matter in head volume conductor modeling. Especially for the MEG, the modeling of skull spongiosa and compacta might be neglected due to the weak effects; the simplification of not modeling white matter anisotropy is admissible considering the complexity and current limitations of the underlying modeling approach.

© 2014 Elsevier Inc. All rights reserved.

## Introduction

Electro- and magnetoencephalography (EEG and MEG) have become important tools in the analysis of brain activity in a variety of applications in both science and medicine, e.g., brain research or clinical analysis. In many of these applications, the aim is to reconstruct the sources inside the brain volume that underlie the measured signal. Therefore, it is necessary to solve an ill-posed inverse problem which requires the simulation of the electric/magnetic field caused by a point-like source inside the brain volume: the so-called forward problem of EEG/MEG (Brette and Destexhe, 2012). The achievable accuracy

in the inverse problem strongly depends on an accurate forward solution. The influence of the head modeling accuracy on the forward solution—and also on the related inverse solution—has been subject to several studies.

Early EEG/MEG source analysis used (multi-layer) sphere models to approximate the human head (de Munck and Peters, 1993), which may have, of course, led to extreme inaccuracies in the forward simulation. As a first step towards more realistic head modeling, the impact of using realistically shaped 3-layer head models distinguishing the boundaries between skin, skull, and a homogenized brain compartment was demonstrated (Brette and Destexhe, 2012). However, such models are still based on a variety of simplifications. The introduction of a homogenized brain compartment inside the inner skull surface neglects the highly conductive cerebrospinal fluid (CSF) (Lanfer et al., 2012a; Ramon et al., 2004; Wendel et al., 2008), whose conductivity is well

* Corresponding author at: Institute for Biomagnetism and Biosignalanalysis, University of Münster, Malmedyweg 15, 48149 Münster, Germany. Fax: +49 251 83 56874.
E-mail address: j.vorwerk@uni-muenster.de (J. Vorwerk).

known and has a negligible inter-individual variability (Baumann et al., 1997). The important effect of modeling the CSF compartment has also been shown in EEG experiments (Rice et al., 2013). Furthermore, a homogenized brain compartment neglects the conductivity differences between gray and white matter as well as the highly anisotropic structure of the white matter (Güllmar et al., 2010; Ramon et al., 2004). In addition, modeling the skull as a closed shell of isotropic conductivity enveloping the brain and the CSF disregards the layered structure of the skull (Akhtari et al., 2002; Dannhauer et al., 2011; Sadleir and Argibay, 2007) and the importance of modeling skull holes and inhomogeneity accurately (Lanfer et al., 2012b; Montes-Restrepo et al., 2013; Ollikainen et al., 1999; Pohlmeier et al., 1997).

Since the MEG is assumed to be less affected by a simplified modeling of the human head, many of the above studies concentrated on the effects of realistic head modeling on the EEG, while only few of them also incorporated MEG effects. Instead, several papers focused on investigating the different sensitivity of the two modalities using realistically shaped 3-layer head models (Ahlfors et al., 2010; Dassios et al., 2007; Goldenholz et al., 2009). Nevertheless, scenarios exist where it is unclear whether a more detailed simulation of volume conduction effects can still be omitted, e.g., when a combined inverse analysis of EEG and MEG is desired. A combined analysis of EEG and MEG is highly worthwhile to account for the different sensitivities of the two modalities particularly with regard to the reconstruction of source orientation and depth. Here, the EEG is in many cases helpful to recover the radial part of the source orientation. Thus, a combined analysis helps to achieve the goal of reliably identifying and localizing sources of arbitrary orientation and depth. Applications where this is desirable are, e.g., epilepsy diagnosis (Aydin et al., 2014; Iwasaki et al., 2005; Salayev et al., 2006), evoked response analysis, and connectivity studies (Astolfi et al., 2005; Lin et al., 2009).

The goal of this study was to investigate the influence of modeling/ not modeling different conductive compartments and features of the human head—skull compacta, skull spongiosa, CSF, gray matter, white matter, and white matter anisotropy—in the creation of a volume conductor on both EEG and MEG forward solutions and to compare them with respect to their impact. Furthermore, we set these effects in relation to the numerical error and to the results of previous studies dealing with the influence of volume conductor modeling on the EEG/MEG forward solution.

By applying a state-of-the-art finite element approach to solve the EEG/MEG forward problem in our simulations, we were able to also include head compartments of complicated shape. Accordingly, we created highly realistic head models and used realistic sensor configurations. We distributed sources with a high, regular density in the gray matter compartment and chose their orientation perpendicular to the gray/white matter interface. Following this, we calculated the effects of the changed volume conduction on forward solutions caused by neglecting the conductivity differences between certain head compartments. Therefore, we used difference measures designed to differentiate between topography and magnitude changes. We then visualized the results on an inflated brain surface to depict the spatial distribution of these changes for both EEG and MEG. The differentiation between topography and magnitude effects is of high importance since they strongly differ in their impact on inverse solutions. Additionally, we presented these effects in special diagrams, known as heat maps, where we related their strength to parameters characteristic of the source location. These analyses allowed us to estimate the influence of simplifications in head model creation on the investigation of activity originating in certain brain regions. Thereby, we were able to show the high importance of accurate volume conductor modeling for EEG and, to a lesser degree, for MEG forward solutions and worked out a guideline for volume conductor modeling in EEG and MEG source analysis. We found the consideration of the highly conductive CSF and the distinction of gray/white matter conductivity differences to be the most important modeling steps.

## Materials and methods

### Model generation

To construct a realistic, high-resolution volume conductor with anisotropic white matter, T1-weighted (T1w-), T2-weighted (T2w-), and diffusion-tensor (DT-) MRI scans of a healthy 25-year-old male subject were acquired with a 3 T MR scanner (Magnetom Trio, Siemens, Munich, Germany) using a 32-channel head coil. For the T1w-MRI, we used an MP-RAGE pulse sequence (TR/TE/TI/FA = 2300 ms/3.03 ms/ 1100 ms/8°, FOV = 256 × 256 × 192 mm, voxel size = 1 × 1 × 1 mm) with fat suppression and GRAPPA parallel imaging (acceleration factor = 2). For the T2w image, an SPC pulse sequence (TR/TE = 2000 ms/307 ms, FOV = 255 × 255 × 176 mm, voxel size = 0.99 × 1.0 × 1.0 mm interpolated to 0.498 × 0.498 × 1.00 mm) was used. MR images were resampled to 1 mm isotropic resolution. DT-MRIs (DTI) were acquired with the standard Siemens pulse sequence ep2d_diff (TR/TE = 7700 ms/89 ms). Geometry parameters were: FOV 220 × 220 × 141 mm, voxel size = 2.2 × 2.2 × 2.2 mm. Seven volumes were acquired with diffusion sensitivity b = 0 s/mm² (i.e., flat diffusion gradient) and 61 volumes with b = 1000 s/mm² for diffusion weighting gradients in 61 directions, equally distributed on a sphere. Seven additional data sets with only flat diffusion gradients and reversed spatial encoding gradients were acquired for distortion correction according to Ruthotto et al. (2012). The T2w-MRI was registered onto the T1w-MRI using a rigid registration approach and mutual information as cost-function as implemented in the FSL-toolbox (http://fsl. fmrib.ox.ac.uk/fsl/fslwiki/FSL). The skin, skull compacta, and skull spongiosa were segmented by applying a gray-value based active contour approach (Vese and Chan, 2002). Subsequently, the segmentation was manually corrected and, because of the importance of modeling skull holes for source analysis (Oostenveld and Oostendorp, 2002; van den Broek et al., 1998), the foramen magnum and the two optic canals were correctly modeled as skull openings. Following the advice of Lanfer et al. (2012b), the model was not cut off directly below the skull but realistically extended at the neck. Curry (http://www. neuroscan.com) was used to extract high-resolution surfaces of skin, skull compacta, and skull spongiosa. A Taubin smoothing was applied to remove staircase-like effects (Taubin, 1995). The FreeSurfer-toolbox (https://surfer.nmr.mgh.harvard.edu) was then used to segment and extract the cortex surface and the gray/white matter interface.

In order to be able to apply a constrained Delaunay tetrahedralization (CDT), all obtained surfaces were checked for intersections and those found were corrected by flattening the inner surface, ensuring a minimal distance between all surfaces. The CDT was executed using TetGen (http://www.tetgen.org); the resulting mesh consists of 984,569 nodes and 6,107,561 tetrahedral elements (Fig. 1a). Additionally, a mesh with a higher resolution of 2,159,337 nodes and 13,636,249 elements was constructed using the same surfaces in order to be able to compare numerical errors and modeling errors later on. The conductivities used in our study were chosen according to Table 1 (Akhtari et al., 2002; Baumann et al., 1997; Dannhauer et al., 2011; Ramon et al., 2004).

To construct anisotropic conductivity tensors in the white matter, after a first affine registration for eddy current correction, the DW-MRIs were corrected for susceptibility artifacts using a novel reversed gradient approach based on the acquired images with flat diffusion gradient that leads to a diffeomorphic, smooth, and thus physically reasonable transformation (Ruthotto et al., 2012). Finally, the corrected DW-MRIs were registered to the T2-MRI using a rigid transformation. Following the effective medium approach by Tuch et al. (2001) that has been positively validated in a variety of studies (Butson et al., 2007; Chaturvedi et al., 2010; Oh et al., 2006; Tuch et al., 2001), we deduced conductivity tensors $\sigma$ from the diffusion tensors $D$ using the linear relationship $\sigma = sD$. Instead of using the theoretically derived scaling factor $s$ as proposed by Tuch et al. (2001), we chose to compute $s$ empirically adapting the approach used in Rullmann et al. (2009). We

**Fig. 1.** a) Sagittal cut through the volume conductor model (white matter shown in light gray, gray matter in dark gray, CSF in light blue, skull compacta in dark blue, skull spongiosa in red, and skin in yellow) b) Fractional anisotropy visualized on an axial slice of the T1-MRI c) Sources visualized on the brain surface.

dispensed the modeling of gray matter anisotropy due to the severe influence of partial volume effects at the resolutions achieved in a 3 T MR scanner and the only weak radial cortical anisotropy (Fig. 4 in (Heidemann et al., 2010), Fig. 1b). Thus, the computation of $s$ reduced to:

$$s = \sigma_{wm}^{iso} \left( \frac{d_{wm}}{N_{wm}} \right)^{-1}$$

$d_{wm}$ is the sum over the product of all diffusion tensor eigenvalues corresponding to voxels classified as white matter, and $N_{wm}$ is the number of these tensors. This approach ensured that the mean conductivity of the anisotropic white matter fits that of isotropic white matter. Finally, we assigned each element the conductivity tensor corresponding to its barycenter.

### Setup of the head models

To investigate the influence of considering/not considering conductivity differences between the different compartments on the accuracy of the forward simulation, we introduced head models with a differently detailed discrimination of these compartments. Except for the highly resolved model 6CA_hr, we did not change the finite element mesh and thus the geometrical structure of the head model, i.e., the influence of geometrical errors was not examined here.

We constructed five differently detailed head models based on the finite element mesh with the lower resolution (i.e., 984,569 nodes). To follow the steps in which one would usually extend a head model to achieve a more realistic representation, we started from the commonly used 3-compartment head model with homogenized isotropic skull and brain compartments, which in our case was extended by the realistic modeling of skull holes that were already included as a necessity of our approach not to change the geometrical representation of the volume conductor (model 3CI in Table 1). We extended this model by the distinction of further compartments, namely the CSF (model 4CI in Table 1), gray and white matter separation (model 5CI in Table 1),

skull compacta and spongiosa separation (model 6CI in Table 1), and finally by the inclusion of white matter anisotropy (model 6CA in Table 1). Head model 6CA_hr was based on the highly resolved mesh (2,159,337 nodes) and served as a reference to estimate the numerical error. Due to the fact that we assigned the anisotropic conductivity tensor according to each element's barycenter, this error contained not only the numerical error caused by the different model resolutions, but also the effect of the possibly slightly different subsampling of tensors. Since we expected the numerical error to dominate, we simply called it numerical error.

### Sensor setup

We used realistic sensor configurations for both EEG and MEG. The positions of 74 electrodes (10–10 system) were digitized using a Polhemus device and projected onto the skin surface. A 275-channel whole head MEG gradiometer sensor configuration (CTF Omega 2005 MEG by MISL, http://www.vsmmedtech.com/hardware.html) was modeled and a rigid transformation to the head model was calculated using the positions of head localization coils inside the MEG and the positions of fiducials placed at the corresponding positions during the MRI recordings.

### Finite element forward approach

We applied the finite element method (FEM) to solve the forward problem due to its ability to deal with complex geometries, e.g., skull holes or the strongly folded cortex surface, and tissue conductivity anisotropy without serious influence on computation speed and accuracy. Different approaches to modeling the source singularity when using FE methods have been investigated: Examples from the literature include the subtraction approach (Drechsler et al., 2009), the partial integration direct approach (Schimpf et al., 2002), and the Venant direct approach (Buchner et al., 1997; Wolters et al., 2007). In our study, we decided to use the Venant approach based on comparisons of the performance of these approaches, which suggest that for sufficiently regular meshes,

**Table 1**
Overview of the compartment conductivities, the conductive features of the different head models (I is considered, - is disregarded,: is further divided, and A is anisotropic), and their resolution.

| Compartment | $\sigma$ S/m | 3CI | 4CI | 5CI | 6CI | 6CA | 6CA_hr |
|---|---|---|---|---|---|---|---|
| Brain | 0.33 | I | I | : | : | : | : |
| Brain GM | 0.33 | - | - | I | I | I | I |
| Brain WM | 0.14 | - | - | I | I | A | A |
| CSF | 1.79 | - | I | I | I | I | I |
| Skin | 0.43 | I | I | I | I | I | I |
| Skull | 0.01 | I | I | I | : | : | : |
| Skull comp. | 0.008 | - | - | - | I | I | I |
| Skull spong. | 0.025 | - | - | - | I | I | I |
| Resolution | #Nodes | 984,569 | 984,569 | 984,569 | 984,569 | 984,569 | 2,159,337 |

the Venant approach yields suitable accuracy over all realistic source locations (Lew et al., 2009; Vorwerk et al., 2012; Wolters et al., 2007). The Venant approach relies on the principle that a current dipole can be approximated by a set of electrical monopoles in the vicinity of the dipole position that matches its dipole moment (and higher moments) and has overall charge zero. The resulting FE approach has a high computational efficiency when used in combination with the FE transfer matrix approach (Wolters et al., 2004) and with an Algebraic MultiGrid preconditioned Conjugate Gradient (AMG-CG) solver (Lew et al., 2009). We used standard piecewise linear basis functions and performed our computations using SimBio (https://www.mrt.uni-jena.de/simbio/index.php/Main_Page).

*Source space construction*

The Venant finite element approach requires special care to be taken in the construction of volume conductor and source space mesh. We chose to place sources with a normal constraint in the gray matter, as it is physiologically plausible (Brette and Destexhe, 2012). Therefore, we had to ensure that the vertex closest to the source position was exclusively part of elements belonging to the gray matter, the so-called Venant condition. Otherwise, the examined effects of conductivity changes in the neighboring compartments, i.e., white matter and CSF, might have been corrupted by numerical inaccuracies (Vorwerk, 2011). Starting from 129,640 regularly distributed source positions on the gray/white matter surface, we calculated a surface normal at each position and fixed it as the source orientation (Fig. 1c). Then, all vertices in the gray matter compartment fulfilling the Venant condition were computed and the source positions were moved into the direction of the next valid node, until this node was the node closest to the source position. Thereby, we ensured that our results were not disturbed by numerical inaccuracies.

*Difference measures*

When comparing solutions of the EEG/MEG forward problem calculated with the different head models, two possible types of effects have to be considered: topography and magnitude changes. While topography changes, i.e., changes in the shape of the potential/field, might in praxis lead to a wrong localization of reconstructed sources, magnitude changes might lead to a wrong reconstruction of source magnitudes. To distinguish these errors, two difference measures were applied in our evaluations, namely the relative difference measure (RDM) and the logarithmic magnitude difference measure (lnMAG) (Güllmar et al., 2010; Meijs et al., 1989):

$$RDM(u, u_{ref}) = \left\| \frac{u}{\|u\|_2} - \frac{u_{ref}}{\|u_{ref}\|_2} \right\|_2$$

$$lnMAG(u, u_{ref}) = \log \frac{\|u\|_2}{\|u_{ref}\|_2}$$

$u$ and $u_{ref}$ denote the vectors of simulated sensor values for test and reference solution, respectively. While the RDM is a normalized $l_2$-difference and indicates the topography change compared to a reference solution, the lnMAG measures the ratio between the overall magnitudes of two solutions, where we defined (signal) magnitude as the $l_2$-norm over all sensor values. The lnMAG is 0 when the magnitudes are equal, and a positive value corresponds to an increased magnitude in comparison to the reference solution. Thus, a smaller absolute value of the lnMAG correlates to a lower difference in signal magnitude. Compared to the commonly used MAG, it has the advantage of being symmetric around 0 so that the magnitude of increases and decreases in signal strength can directly be compared. The absolute values of the lnMAG are sometimes of less interest, e.g., if one only wants to compare the magnitude of reconstructed sources at different locations. In such

scenarios, a large variance of the lnMAG, i.e., the ratios of signal magnitudes of sources at different positions are strongly distorted, might easily lead to misinterpretations. Thus, we also took the width of the distribution of the lnMAG differences into account. The RDM is bounded between 0 and 2, where a smaller value corresponds to a lower difference in signal topography. Dannhauer et al. (2011) showed that a higher RDM is related to a worse source localization.

*Effect evaluation/visualization*

We used different kinds of diagrams to display the overall distribution of certain quantities (RDM, lnMAG, signal magnitude, etc.). To visualize the effect of both single steps of head model refinement and the difference in relation to the reference model, we plotted cumulated relative frequencies (see, e.g., Fig. 4). These diagrams have the advantage that the shape of the plotted curve is less dependent on the choice of the interval length than in common histograms. Furthermore, we used 2D histograms to show the dependency of the magnitude of the effect measures on a certain model parameter and previous to this to analyze the interdependency between the model parameters used here. To create these plots, a matrix was calculated where each entry determined the frequency of values that are both inside a specific interval on ordinate and abscissa. This distribution was visualized using heat maps, and, for the sake of better recognizability, each column was scaled by the inverse of its maximum (i.e., normalized to a maximum of 1) (see, e.g., Fig. 7). The heat maps provide more information than more common graphical representations, e.g., box plots or floating mean plots, since they allow a more detailed overview of the effect distribution and it is also possible to recognize weak dependencies that might be overlooked in other modalities. Common graphs were created using gnuplot (http://www.gnuplot.info), heat maps were created using MATLAB.

*Visualization*

For visualization purposes, an inflation of the gray/white matter surface was created using BrainVISA (http://www.brainvisa.info). On the resulting surface we depicted the values of effect measures or parameters (see, e.g., Fig. 3). In Fig. 2, the inflation process is presented. This visualization allowed us to classify the brain regions that were most affected or not affected by the refinement steps. In addition to the color-coded visualization of effects, we calculated the curvature of the original surface and displayed it underneath the effect results to allow better identification of brain regions. A positive curvature, which roughly corresponds to gyri, is shown in light gray, a negative curvature is shown in dark gray (Fig. 2). The most tangential source orientations were thus roughly achieved around the intersection between light and dark gray and the most radial source orientations in the middle of the light and dark gray regions. We introduced an increasing transparency for smaller values so that the underlying curvature is still visible in the plots (see, e.g., Figs. 8b and d). All visualizations were carried out using SCIRun (http://www.sci.utah.edu/cibc-software/scirun.html).

*Spatial measures*

We used the quantities signal magnitude, i.e., $\|u\|_2$, the distance between a source position $x$ and the inner skull surface, i.e., $\min_{y \in Skull} \|x - y\|_2$, which we denote as source depth, and the median of the distances between a source position and the sensor positions as an indicator for the sensor distance/coverage of a source to quantitatively describe the spatial effect distributions. For each refinement step of the head model we then created heat maps with one of these properties on the x-axis and with one of the difference measures on the y-axis.

To be able to set up heat maps that allow for a more distinct view on the effects of model refinement, we searched for parameters that describe certain characteristics of sources so that the diagram depicts the effect as a function of these parameters. A natural candidate to
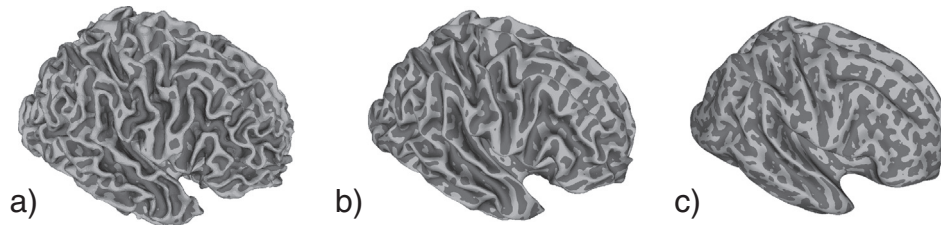
**Fig. 2.** Inflation of the gray/white matter surface: a) Segmented gray/white matter surface b) after half of the inflation steps and c) final result on which effect surface plots are presented.

discriminate source positions and orientations is the overall signal magnitude. For the EEG it is mainly correlated with the depth of the source and its sensor coverage, while it is also strongly dependent on the source orientation for the MEG (cf. EEG and MEG signal magnitude section). A drawback of using the signal magnitude as a parameter is that due to the dependency on both orientation and sensor coverage, less insight into the spatial distribution of the effects is gained. A second possible parameter we considered was the distance between a source position and the inner skull surface. It can be interpreted as an analog to the source depth/eccentricity in sphere models and thus gives a good impression of the relation between effect strength and source position. A drawback of this measure is that no information about sensor coverage is contained, since, e.g., also sources at the base of the frontal lobe may be very close to lower parts of the skull, while sensor coverage is much worse there than for sources at the superior parts of the brain. A possible way to circumvent this problem is to concentrate on distances relative to the sensor positions instead of those relative to a model surface. We chose to take into account the median of the distances between a source position and the sensors/coils as a parameter. It can be interpreted as an intermediate between the two previously proposed measures, taking both the sensor coverage and the source depth into account. Nevertheless, the spatial differentiation by this parameter is less clear than by the distance to the inner skull surface, on which we therefore mainly relied.

## Results

We calculated forward solutions for the models presented in Table 1 and the respective source space introduced in the Materials and methods section. RDM and lnMAG differences were computed for each source position, both relative to the reference model and between models with one refinement step in between. Furthermore, we calculated the signal magnitude for each source position in all models. On this basis, we performed a series of different evaluations to achieve a decent overview of effect magnitudes.

### EEG and MEG signal magnitude

Fig. 3 shows the distribution of the signal magnitude (relative to the maximum for the respective model) plotted on the brain surface for EEG (upper row) and MEG (lower row) computed in models *3CI* (left column) and *6CA* (right column). These plots underline the different sensitivities of EEG and MEG, an important parameter by which to interpret effect results in our later investigations. The EEG signal magnitudes in Figs. 3a and b have their local peaks for superficial sources close to or on the gyral crowns, where sources are very close to the electrodes, and decrease continuously when going to deeper source positions. We found the weakest EEG signal magnitudes for sources in sulcal valleys. The *3CI* distribution (Fig. 3a) showed large areas of above 90% relative
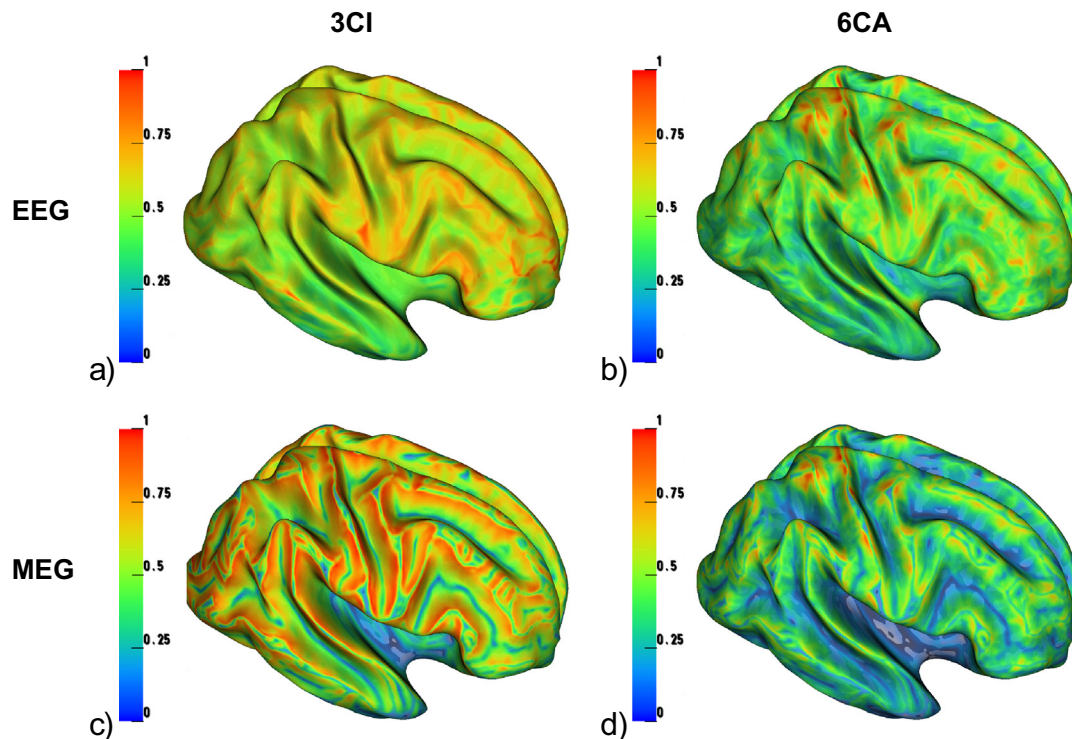


**Fig. 3.** Signal magnitude (in $V^2$/$fT^2$) relative to its maximum for the respective model for EEG (upper row) and MEG (lower row) computed in models *3CI* (left column) and *6CA* (right column).

signal strength and hardly any areas below 22%, while the *6CA* distribution (Fig. 3b) was less smooth and had a broad range with only a few small areas of above 90% relative signal magnitude and large areas of below 22%. In contrast, for the MEG (Figs. 3c and d) the signal decay into the depth was stronger than for the EEG and the signal magnitude was very weak on a thin line on gyral crowns and a broader line in sulcal valleys, where sources are quasi-radial. A small displacement of the source from the thin line at the gyral crown caused the orientation to change strongly towards a more tangential direction and the signal rapidly increased to its local peak value. As for the EEG, the full *6CA* head model (compare Figs. 3c and d) led to a more scattered sensitivity profile. Even though the overall properties described for the *3CI* model were still visible, we could clearly observe the influence of the more detailed conductivity distinction on the local distribution of the signal magnitude, which was no longer nearly exclusively dominated by source depth and orientation.

*Topography and magnitude differences*

As a first evaluation of topography and magnitude changes, we depicted the cumulative relative frequencies of RDM (upper rows) and lnMAG (lower rows) for EEG (Fig. 4) and MEG (Fig. 5), showing the effects between single refinement steps (left columns) and the overall effects of the various models compared to the reference model *6CA_hr* (right columns). This presentation allowed for a first, very general, interpretation of the influence of the distinction of certain conductive compartments on the forward solution. Second, we investigated the inter-dependencies of the different properties, which were used to classify the effects of the model refinement (cf. Setup of the head models) (Figs. 6 and 7). Finally, we used heat maps of RDM and lnMAG as a function of these properties as well as surface plots of the effect measures to identify and classify the brain regions most affected by the model refinements (Figs. 8–15).

We found that the introduction of the CSF had the biggest influence on the EEG forward simulation, both regarding RDM and lnMAG (dark blue lines in Figs. 4a and c). While for the RDM the plot shows that the influence of gray/white matter distinction (red line in Fig. 4a) and white matter anisotropy (light blue line in Fig. 4a) was only slightly smaller, the consideration of the CSF led to by far the biggest effect regarding the lnMAG in absolute values (dark blue line in Fig. 4c). Looking at the variance of the lnMAG effects, we found that for each of these three steps (dark blue, red, and light blue lines) about 90% of the sources lay in an interval with a width of about 0.4 in lnMAG (e.g., the red line in Fig. 4c reaches a cumulated relative frequency of 0.05 at about −0.3 and of 0.95 at about 0.1), which would correspond to a misestimation by a factor of up to 1.5 when comparing the magnitudes of reconstructed sources. In both modalities, the influence of modeling the different skull compartments showed a minor effect (orange lines in Figs. 4a and c), though the effects caused were still higher than the numerical error, i.e., the difference between model *6CA* and *6CA_hr* (green lines in Fig. 4). As Figs. 4b and d show, the effects of the different refinement steps mainly added up and did not cancel each other out.

The RDM results of the MEG simulations were very similar to those of the EEG simulations. Again, distinction of CSF (dark blue line in Fig. 5a) and gray/white matter (red line in Fig. 5a) showed the biggest influence. The magnitude of these effects was nearly identical in this case. The influence of white matter anisotropy was clearly smaller (light blue line in Fig. 5a), while skull modeling (orange line in Fig. 5a) and numerical error (green line in Fig. 5a) were at the same, small, level. Regarding the lnMAG, the effect of gray/white matter distinction (red line in Fig. 5c) was even bigger than that of CSF modeling in absolute values (blue line in Fig. 5c). These effects had opposite signs—a result in line with the increase (CSF added) and decrease (WM added) of the conductivity in large parts of the head. As in the EEG case, the width of the distribution of the lnMAG for the distinction of CSF and gray/white matter, as well as for the inclusion of anisotropy, was in the same range. For all three of these effects, 90% of the sources fell
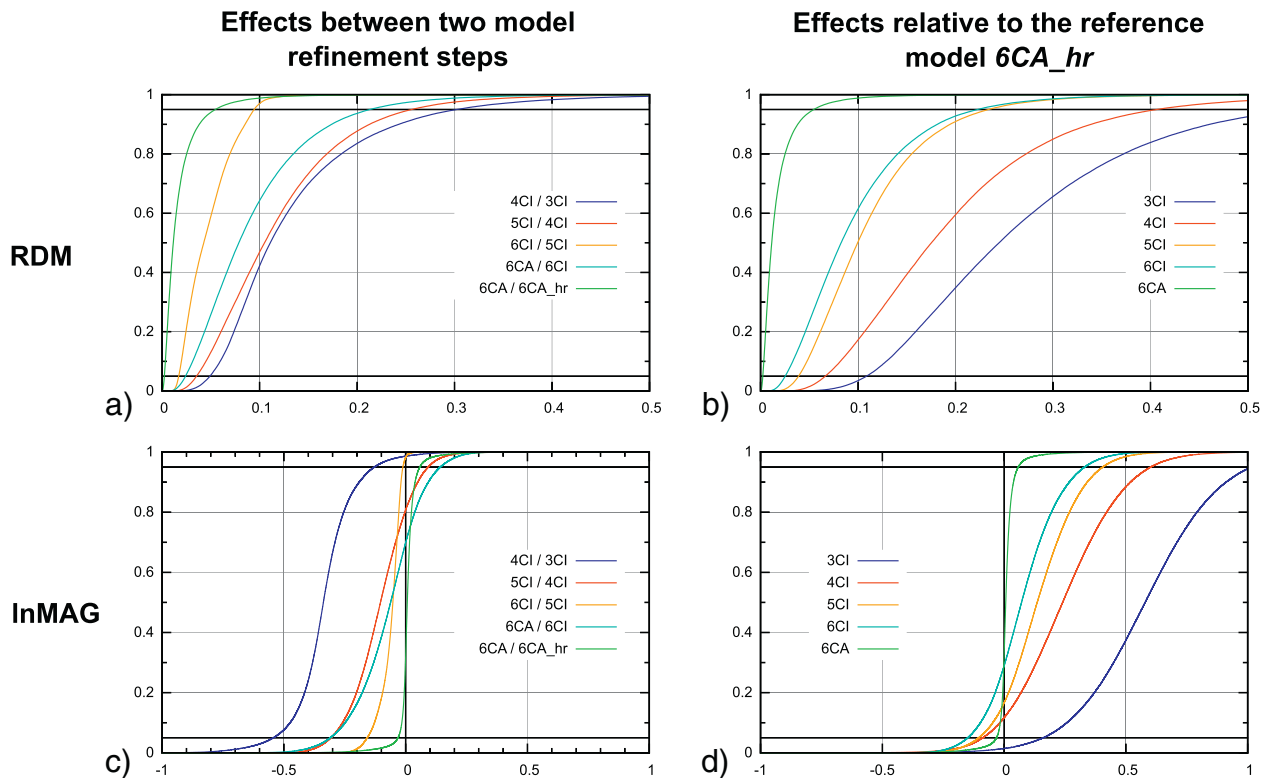


**Fig. 4.** Cumulative relative frequencies for effects induced in EEG. RDM (upper row) and lnMAG (lower row) between two refinement steps (left column) and relative to the reference model *6CA_hr* (right column). The horizontal lines indicate frequencies of 0.05 and 0.95.
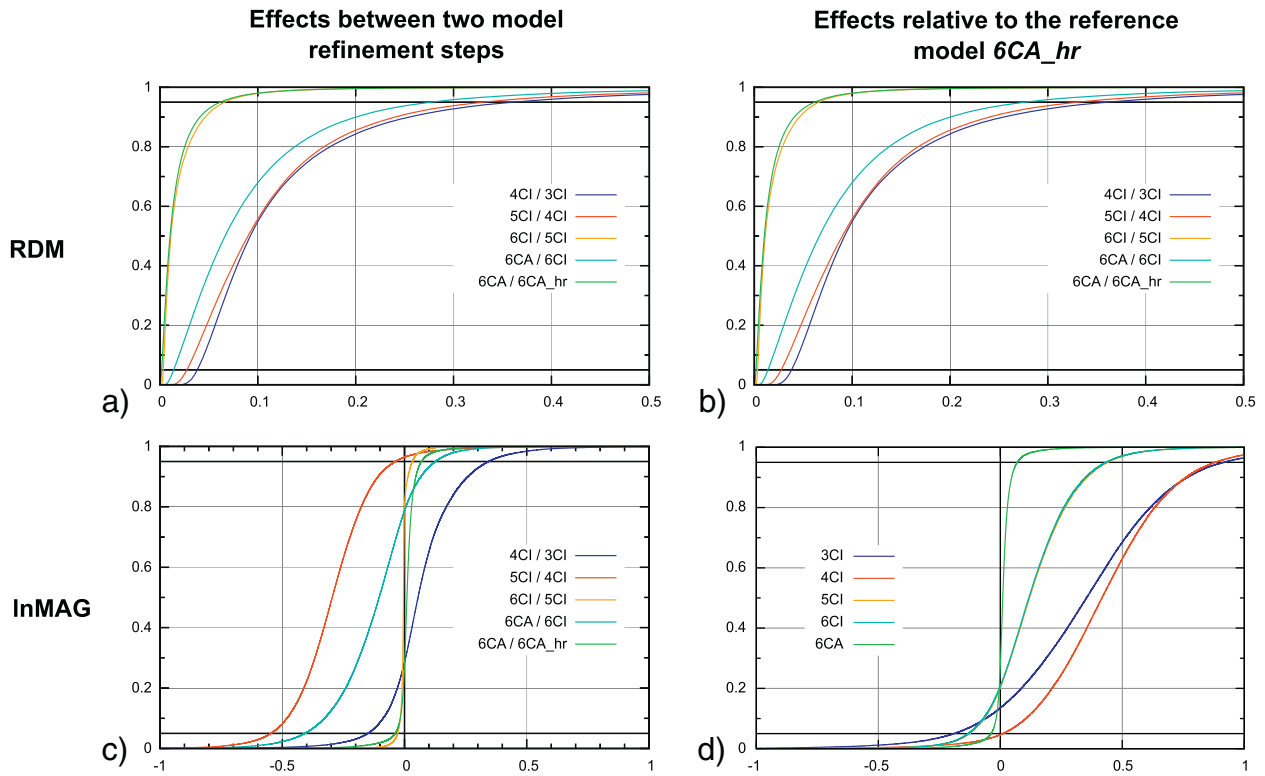
## Effects between two model refinement steps

## Effects relative to the reference model *6CA_hr*

**RDM**

a)

b)

**lnMAG**

c)

d)

**Fig. 5.** Cumulative relative frequencies for effects induced in MEG. RDM (upper row) and lnMAG (lower row) between two refinement steps (left column) and relative to the reference model *6CA_hr* (right column).

within a range of about 0.5 in lnMAG (e.g., the light blue line in Fig. 5c reaches a cumulated relative frequency of 0.05 at about −0.4 and of 0.95 at about 0.1), which would correspond to a misestimation by a factor of over 1.6 when comparing source magnitudes. In comparison, the numerical error would only lead to a factor of 1.1.

Comparing the size of the effects for EEG and MEG, we found that they were at a similar level. This might be counterintuitive at first glance, since one would expect the MEG to be less influenced by conductivity changes, but actually this is a consequence of our approach to choose sources perpendicular to the brain surface so that also quasi-radial and very deep sources were included in the analysis. This part of the sources led to a weak MEG sensor signal, and, thus, small absolute effects directly led to big relative effects. One could have tried to avoid this effect by excluding sources with low signal magnitude or a pre-selection of sources with regard to positions and directions, but this would have increased the possibility of a biased evaluation result. Instead, we chose to include all sources in the analysis, and tried to create visualizations where one can particularly identify the effects of quasi-radial and deep sources.

Finally, we observed that the numerical error in comparison to the highly resolved model *6CA_hr* was smaller than all observed model

effects in both modalities, underlining the high accuracy of the FE approach and model used.

*Evaluation of spatial measures*

The plots of the cumulative relative frequency of RDM and lnMAG already gave a valuable overview of the importance of the different head tissue properties for the EEG and MEG forward problem. However, we wanted to strive for a deeper insight into the relationship of source properties and volume conduction effects. As the following investigations show, this relationship can be further enlightened using the additional measures and visualization means introduced in the Materials and methods section.

The important characteristics of the spatial distribution of the signal magnitude for EEG and MEG are shown in Fig. 3 and have already been discussed in the EEG and MEG signal magnitude section.

In Fig. 6, the median of the distances between a source position and the electrodes (left) and the distance between a source position and the inner skull surface (right) were visualized on the brain surface. In Fig. 6a it can be observed that a high median is mainly given for temporal and

a)                                                          b)
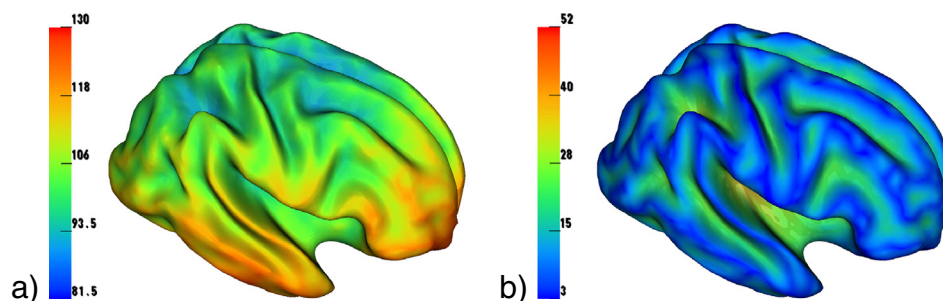
**Fig. 6.** a) Median of the distances between a source position and the electrodes (in mm) b) distance between a source position and the inner skull surface (in mm).

**Signal magnitude (V², y-axis) vs. median of distances to the electrodes (mm, x-axis) for EEG**

**Signal magnitude (fT², y-axis) vs. distance to the inner skull surface (mm, x-axis) for MEG**
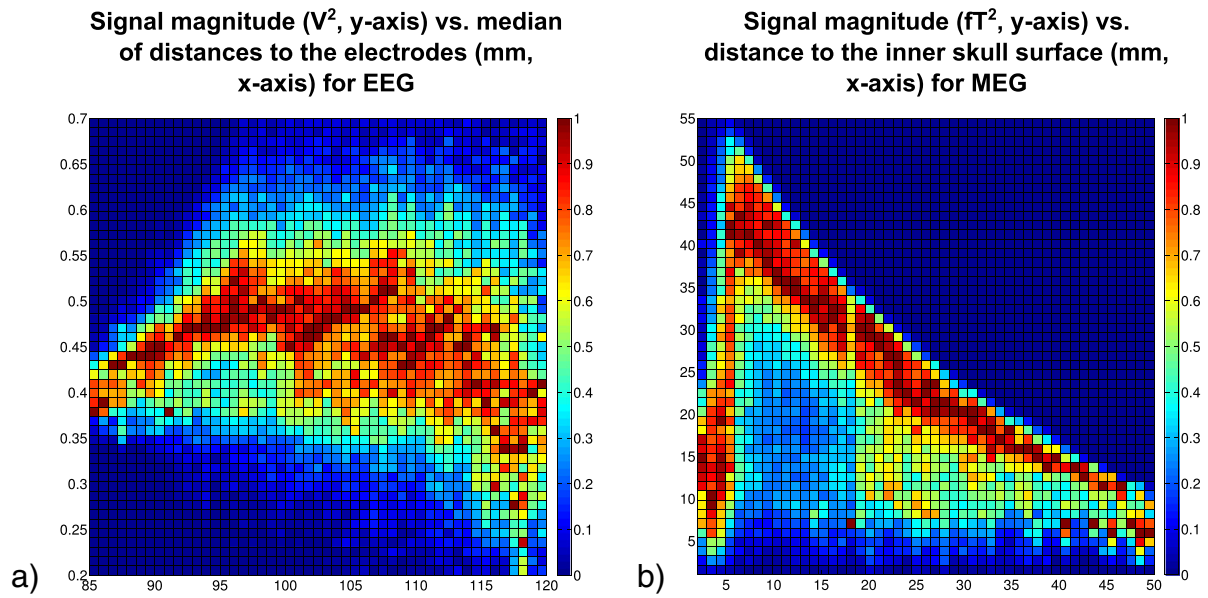


Fig. 7. Signal magnitude (in V²/fT²) computed in model 3CI as a function of a) median of distances between the source position and the electrodes for EEG b) distance to the inner skull surface for MEG.

frontal regions and, in comparison to Fig. 6b, the different focus of this parameter becomes clear.

Fig. 7 shows the dependency of the signal magnitude computed in model 3CI for EEG (left) and MEG (right) on the parameters visualized in Fig. 6. Interestingly, Fig. 7a shows that sources with the smallest and with the largest median have the smallest signal magnitude for the EEG, while those with an intermediate median have the strongest signal. The surface representation in Fig. 6a shows that the latter correspond to more central and superficial sources, which we expected to have the strongest signal. For the MEG, we could identify a set of superficial sources with a weak signal corresponding to quasi-radial sources

on gyral crowns (Fig. 7b, sources with lowest distance to the skull). For both EEG and MEG, Figs. 3a–d and 7b clearly show the decay of the signal magnitude as a consequence of source depth/distance to the inner skull surface. We could not distinguish the quasi-radial sources at sulcal valleys as clearly as those at gyral crowns; they could only be suspected as outliers with low signal magnitude at distances between 18 and 30 mm (Fig. 7b). This can be explained by the differing distance between the sources in the sulcal valleys and the inner skull surface due to the varying sulci depth (causing a blurring in x-direction in Fig. 7b). Furthermore, the difference between the signal magnitude of quasi-radial sources in the sulcal valleys and neighboring sources at

**RDM**

**lnMAG**
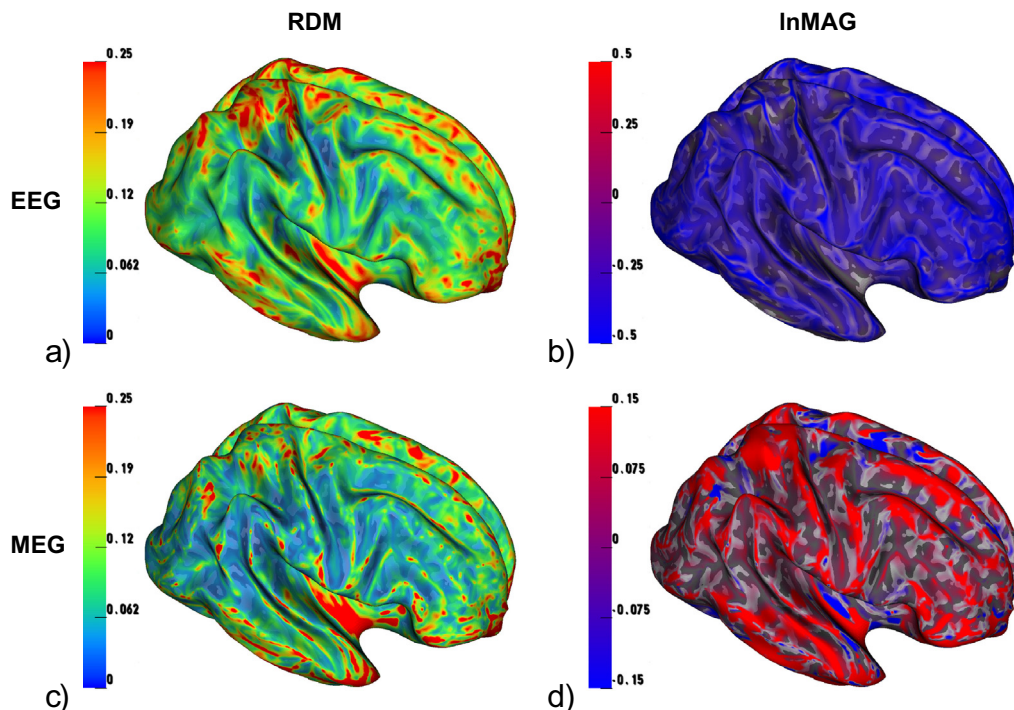


Fig. 8. Effect of CSF distinction—difference between models 4CI and 3CI plotted on brain surface.
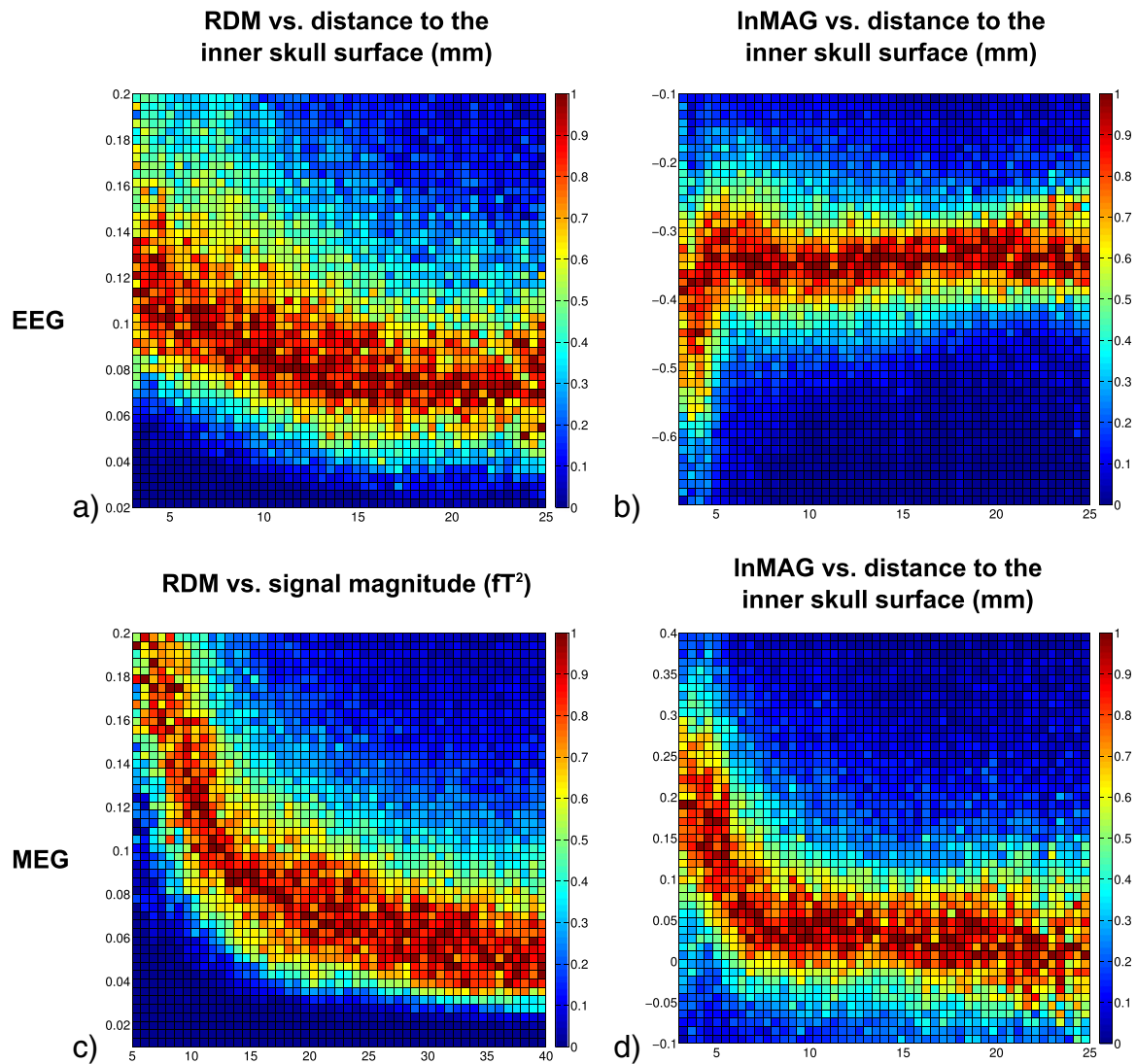
Fig. 9. Effect of CSF distinction—difference between models *4CI* and *3CI* in 2D histogram.

similar depth is much smaller than at gyral crowns (causing a blurring in y-direction).

*Single tissue compartment sensitivity investigation*

Finally, further single tissue sensitivity analyses complemented our investigations. For each refinement step we created a heat map using one of the above proposed parameters for both RDM and lnMAG in addition to the surface plots. In most cases the distance to the inner skull surface was found to be the most meaningful parameter.

*Distinction of CSF*

When evaluating the effect of including the CSF compartment on the EEG, the visual inspection of the surface plots (Figs. 8a and b) was in line with the visualization in the heat maps (Figs. 9a and b) for both difference measures. The lnMAG in Fig. 8b shows a strong decrease of signal magnitude especially for superficial sources (on gyral crowns), which is evident in the diagram in Fig. 9b. We observed a negative lnMAG especially for the most superficial sources, while it was constant at a smaller but still clearly negative level for deeper sources. Such an effect might lead to significant misinterpretations when comparing source magnitudes of superficial and deep reconstructed sources. For the used model, a possible decrease/increase by a factor of up to 1.6 was found. The RDM distribution in Fig. 8a is less clear; we identified

significant effects at the very top of the brain in the vicinity of the inter-hemispheric fissure, in deep areas like the Sylvian fissure, and we found the frontal and temporal poles as well as the inferior temporal lobe to be affected, too. Fig. 8a and especially Fig. 9a show a trend towards lower RDM effects for deeper sources. Here, we found that a lower limit was reached at a depth of about 15 mm below the inner skull surface; for even deeper sources the RDM stayed at a constant level. Even though the trend was clearly recognizable, we observed a considerable variance of effect sizes at all source depths.

We saw a clear effect of the CSF distinction on the MEG in the lnMAG, where the optical impression of increased signal magnitude for superficial sources in Fig. 8d is visible in the heat map plot in Fig. 9d. We found a lower limit reached at a depth of 8 mm below the inner skull surface. As for the EEG, this is especially problematic when comparing the strength of superficial and deeper lying reconstructed sources. The topography of the RDM plot in Fig. 8c is again less clear, but, similar to the EEG case, significant effects were found on some gyral crowns, at the top of the brain, in the Sylvian fissure, at the frontal and temporal poles, and at the inferior temporal lobe. Furthermore, we found a clear correlation of RDM and signal magnitude in Fig. 9c.

*Effect of the distinction between gray and white matter*

For the EEG, we observed strong effects both regarding RDM and lnMAG for the most superficial sources in Figs. 10a and b and 11a and
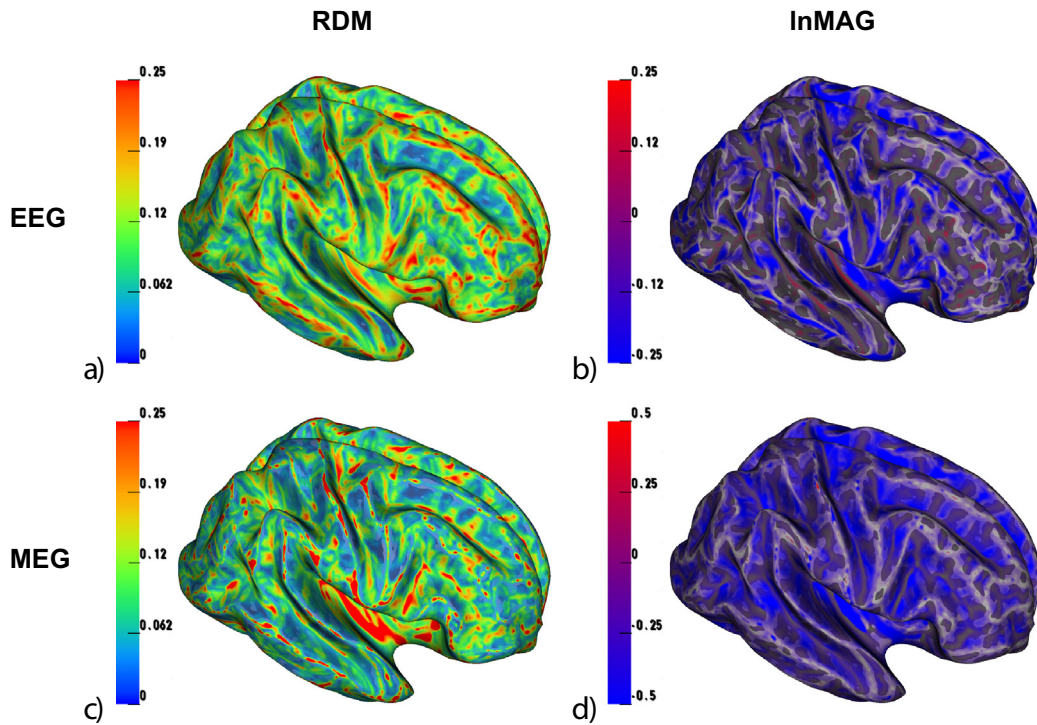
**Fig. 10.** Effect of GM/WM distinction—difference between models *5CI* and *4CI* plotted on brain surface.

b. The surface plot in Fig. 10b shows a strongly decreased magnitude with the lnMAG being partially even below −0.25, and thus exceeding the limit of the color bar, mainly on top of gyri; a finding that is also apparent in the heat map visualization in Fig. 11b. For deeper sources, we found a weaker decrease of EEG signal magnitude (lnMAG between 0 and −0.2, see Fig. 11b). For the few visible areas with an increased magnitude in Fig. 10b, we could find no representation in the heat map plot in Fig. 11b. As seen in Fig. 4, the width of the distribution of the lnMAG effects was as large as for the CSF distinction. Again, especially the differences between very superficial and deeper sources were huge. The spatial distribution of the highest RDM effects was very similar to that of the lnMAG (compare Figs. 10a and b). We found RDM effects above 0.2 for very superficial sources. Visually, we could identify these predominantly on the gyral crowns. For the remaining deeper source positions we still found non-negligible RDM effects with values mainly between 0.05 and 0.1.

The RDM surface plot for the MEG in Fig. 10c shows high effects in areas where sources are suspected to be quasi-radial, again. We furthermore found a clear correlation of these RDM effects to the MEG signal magnitude (similar to Fig. 9c and therefore not shown here). Fig. 11c shows a slight decrease of the effects up to a depth of about 6 mm, followed by an increase for even deeper sources where both the lower bound of effects as well as the mean effects increase. The visualization of the lnMAG in Fig. 10d mainly shows a decrease of MEG signal magnitude, corroborated by the systematic plot in Fig. 11d with nearly all magnitude effects being below 0. At values between −0.1 and −0.3, effects were lowest for superficial sources (as in Fig. 11c, the most superficial quasi-radially oriented sources show bigger effects), getting stronger towards a RDM of −0.4 at a distance of about 1 cm to the inner skull surface and remaining constant for even deeper sources.

*Effect of the distinction between skull spongiosa and skull compacta*

In Figs. 12 and 13, we found notable RDM effects for the EEG mainly at the temporal lobe and its surrounding region, i.e., in a relatively deep area with bad sensor coverage (Fig. 12a). Furthermore, we found some notable topography changes at the very top of the brain. The same

locations were affected when turning to the lnMAG, finding a moderate decrease of signal magnitude (Fig. 12b). Since the areas with a larger median in Fig. 6a strongly correlate to the affected areas in Figs. 12a and b, we used this as a parameter for computing meaningful heat maps. We found that the magnitude of the RDM and lnMAG effects clearly increased with the median of the distances to the electrodes (Figs. 13a and b), showing that the spatial measure used was able to resolve the effects in the visually identified areas as desired. As we found lnMAG effects of up to −0.15 in temporal areas (Fig. 12b), we conclude that using a head model that does not include the distinction between skull spongiosa and compacta might lead to an underestimation of source strength up to a factor of 1.17 when comparing reconstructed sources in temporal areas to those in brain areas with negligible lnMAG effects.

Figs. 12c and d and 13c and d clearly show that the impact of skull spongiosa/compacta distinction was by far weaker for the MEG, which was an expected result. We found a weak influence on the topography for deep sulcal sources (Fig. 12c) in combination with a positive lnMAG (Fig. 12d). This was more pronounced in sulci at the pole of the temporal lobe, in the Sylvian fissure, and in some areas at the base of the frontal lobe. The only parameters that correlated with these small effects were the median of the distances between the source position and the MEG sensors (RDM increases with median in Fig. 13c) and the MEG signal magnitude (Fig. 13d showing a tendency towards a slightly negative lnMAG for weak sources).

*Effect of white matter anisotropy*

Figs. 14a and c (surface plots) and 15a and c (heat maps) show the RDM changes due to white matter anisotropy. For both EEG (Figs. 14a and 15a) and MEG (Figs. 14c and 15c), we found the most significant topography changes for sources in sulcal valleys and on gyral crowns. The heat map for the EEG results in Fig. 15a shows RDM effects mainly between 0.02 and 0.1 at all source depths. A slight trend towards higher effects for deeper sources could be observed, but this was not as distinct as for the other refinement steps. The RDM heat map for the MEG in Fig. 15c shows a clear correlation between signal magnitude and
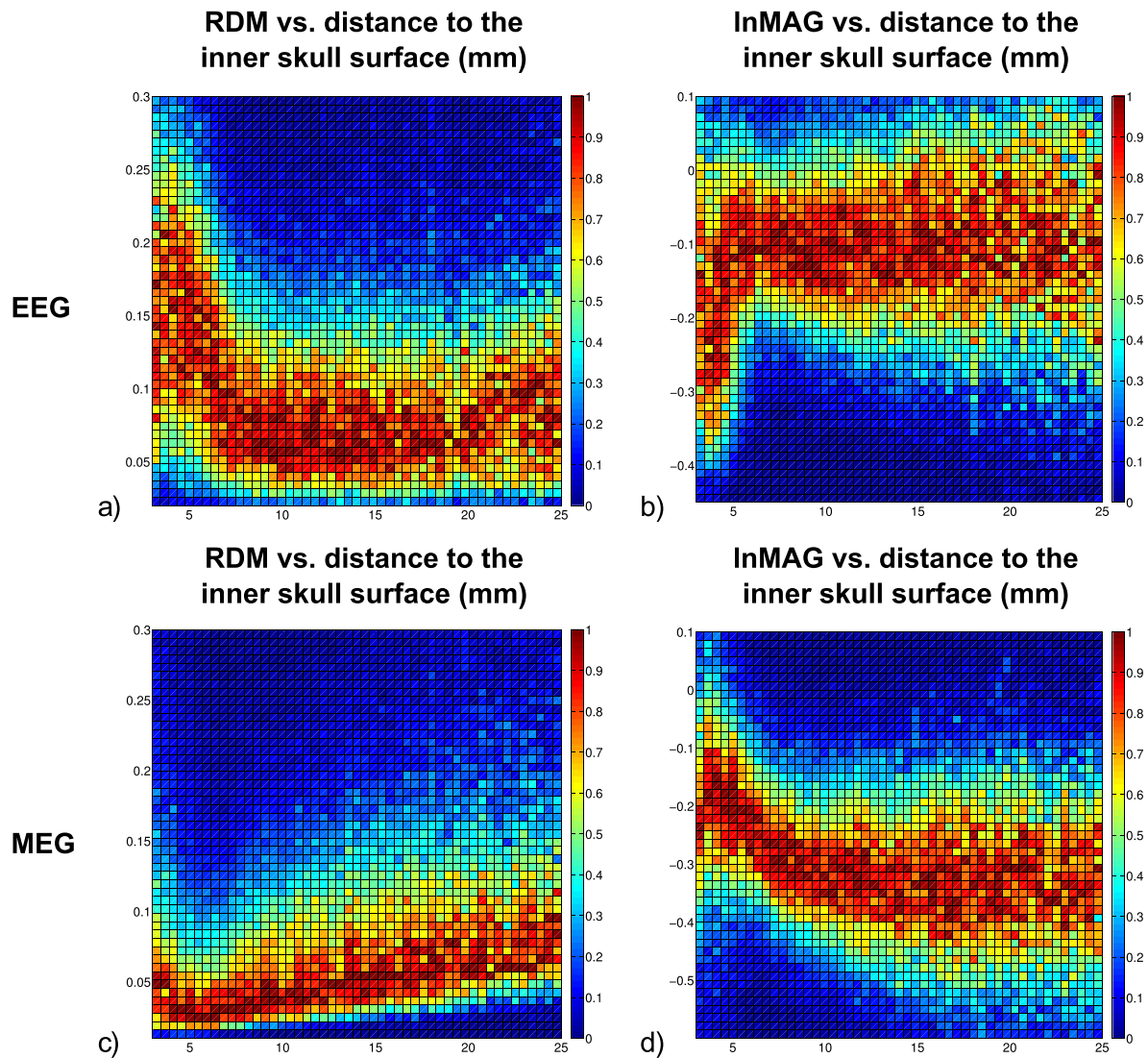
**RDM vs. distance to the inner skull surface (mm)**

**lnMAG vs. distance to the inner skull surface (mm)**

**RDM vs. distance to the inner skull surface (mm)**

**lnMAG vs. distance to the inner skull surface (mm)**



**Fig. 11.** Effect of GM/WM distinction—difference between models *5CI* and *4CI* in 2D histogram.

topography effect, underlining the visual finding of strongest effects for quasi-radial sources.

For both EEG and MEG we found very similar effects with regard to the lnMAG, where the visual impression obtained from Figs. 14b and d was in line with the heat maps in Figs. 15b and d. Minor effects could be reported for the most superficial sources with an lnMAG varying between −0.1 and 0.1 in both modalities. For deeper sources, we found a continuous decrease of signal magnitude in comparison to the *6CI* model, an effect which was less strong for the EEG than for the MEG (Figs. 15b and d).

**Discussion**

In this study we evaluated the influence of modeling/not modeling different conductive head compartments on the finite element forward solution for both EEG and MEG. Our results helped to formulate a guideline for EEG and MEG forward modeling.

We showed that the CSF is one of the most important compartments to be modeled. Especially for superficial sources, modeling the CSF compartment had a large influence on the signal topography for the EEG (Figs. 4a, 8a, 9a) and for the MEG (Figs. 5a, 8c, 9c), while it had a much larger influence on the signal magnitude in EEG (Figs. 4c, 8b, 9b) than in MEG (Figs. 5c, 8d, 9d). In both modalities the distribution of the lnMAG

had a large width. The huge effect for the EEG can easily be explained by the strong increase of conductivity between sources and sensors causing a shunting effect, while the effect for the MEG is probably due to the strong volume currents in the now highly conductive CSF compartment. These were visualized by Wolters et al. (2006), underlining the need for an accurate modeling of this volume.

While our work is a computer simulation sensitivity study and we did not validate effects in real experiments, first validation studies investigating the effects of CSF modeling can be found in the literature and are in line with our results. Rice et al. (2013) showed in EEG experiments that brain shift and the resulting small changes in CSF layer thickness, induced by changing the subject's position from prone to supine, have a significant effect on the EEG in several standard visual paradigms. They describe a local increase of signal magnitude when decreasing the thickness of the CSF by changing the subject's position. This effect is consistent with our finding of a decreased signal magnitude due to the distinction of the CSF. Bijsterbosch et al. (2013) investigated the effect of head orientation on subarachnoid CSF distribution and conclude that minor differences in local CSF thickness are likely to significantly affect the accuracy of EEG source localization techniques. In a further experimental validation study, Bangera et al. (2010) found that the inclusion of CSF as well as brain anisotropy in the forward model is necessary for an accurate description of the electric field inside the skull.
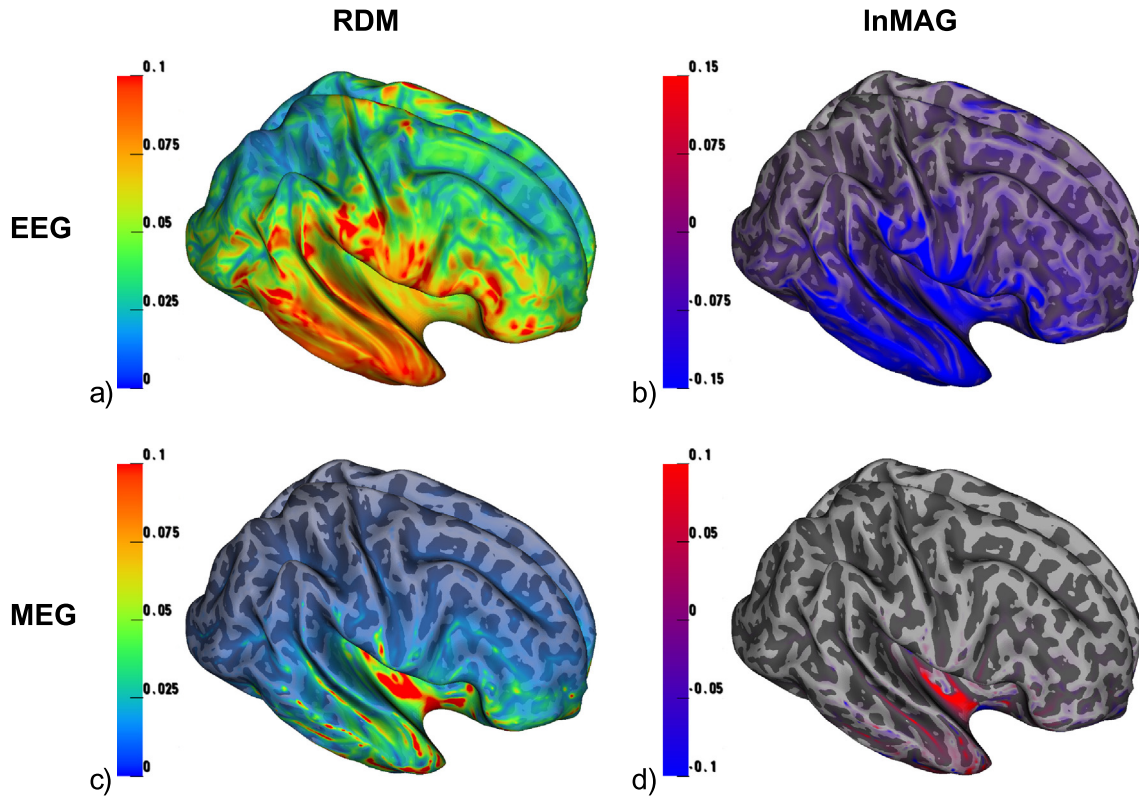
**Fig. 12.** Effect of spongiosa/compacta distinction—difference between models *6CI* and *5CI* plotted on brain surface.

The conductivity of human CSF at body temperature is well known, it was measured to be 1.79 S/m with a low inter-individual variance (Baumann et al., 1997; average over 7 subjects, ranging in age from 4.5 months to 70 years, with a standard deviation of less than 1.4% between subjects and for frequencies between 10 and 10,000 Hz). Thus, the CSF conductivity is one of the best-known parameters in the modeling process giving a further reason for modeling the CSF. The influence of modeling the CSF on forward solutions was also investigated in other computer simulation studies (Ramon et al., 2004; Vallaghe and Clerc, 2009; Wendel et al., 2008), even though the models used, as well as the evaluation methods, differ strongly. In this work we investigated both the influence on EEG and MEG for realistic multi-sensor caps and added a more systematic evaluation of the CSF effect. The examination of the CSF effects in this study confirms and elaborates upon the previous studies, which also observed the decrease of signal amplitudes for the EEG.

Furthermore, we showed that the effect of the gray/white matter distinction is nearly as strong as that of the CSF inclusion in both modalities (Figs. 4a and c, 5a and c), especially with regard to signal magnitude (Figs. 4c, 5c). This stresses the strong effect of conductivity changes in the vicinity of the source (Haueisen et al., 2000). While the EEG was most affected for superficial sources both with regard to topography and magnitude (Figs. 10a and b, 11a and b), we found a stronger decrease of signal amplitude for deep sources than for superficial ones for the MEG (Figs. 10d, 11d). Here, strongest topography effects were found for the most superficial sources and for deeper sources (Figs. 10c, 11c). For the MEG, Figs. 8d and 10d show that the areas most affected by the magnitude effects of these two steps do not overlap, but are mainly disjoint. This was underlined by the distribution of the magnitude effects in relation to the distance to the inner skull (Figs. 9d, 11d), showing the clearly different depth dependency for adding the CSF and gray/white matter distinction. As for the CSF compartment, the gray/white matter distinction induced a conductivity change for a large volume, explaining the strong effect on the signal magnitude.

To the best of our knowledge, only relatively few publications have investigated the effect of the (isotropic) distinction between gray and white matter, even though Haueisen et al. (2000) demonstrated the significant effect of local conductivity changes around the source. The results of Haueisen et al. (1997) suggest a strong change of the signal topography and magnitude for both EEG and MEG when the white matter conductivity is chosen in the range of the gray matter conductivity. From the results presented, it can be concluded that the strength of this effect is slightly lower than the effect of the CSF modeling in *4CI* vs. *3CI* comparisons, which is supported by our findings. Here, our systematic evaluation adds important information about the locations of the most affected sources compared to the single source scenario evaluated by Haueisen et al. (1997), as described previously. Ramon et al. (2004) also found a decrease of the scalp potentials, i.e., the EEG signal, due to the introduction of gray and white matter compartments of differing conductivities, even though the magnitude of the decrease was not further classified. Van Uitert et al. (2004) found the conductivity of white and gray matter to appear especially influential in determining the magnetic field and showed that using a too high white matter conductivity, as it is of course done when not distinguishing between gray and white matter, leads to both high forward and inverse errors.

Compared to the previous two steps, the distinction of skull compartments of different conductivity only showed comparatively weak effects on the EEG (Figs. 4a and c) and nearly no effect on the MEG (Figs. 5a and c). We mainly found the temporal lobe and its surrounding area affected in the EEG both with respect to topography and magnitude (Figs. 12a and b), which might be due to bad sensor coverage. The effect on the MEG was even weaker; it could almost exclusively be seen for deep sources in sulcal valleys (Figs. 12c and d). The relatively small impact of skull spongiosa and compacta distinction was probably partly due to the use of an already optimized conductivity value for the homogenized skull compartment that represents the best fit to the realistic spongiosa/compacta scenario (Dannhauer et al., 2011; Stenroos et al., 2014).
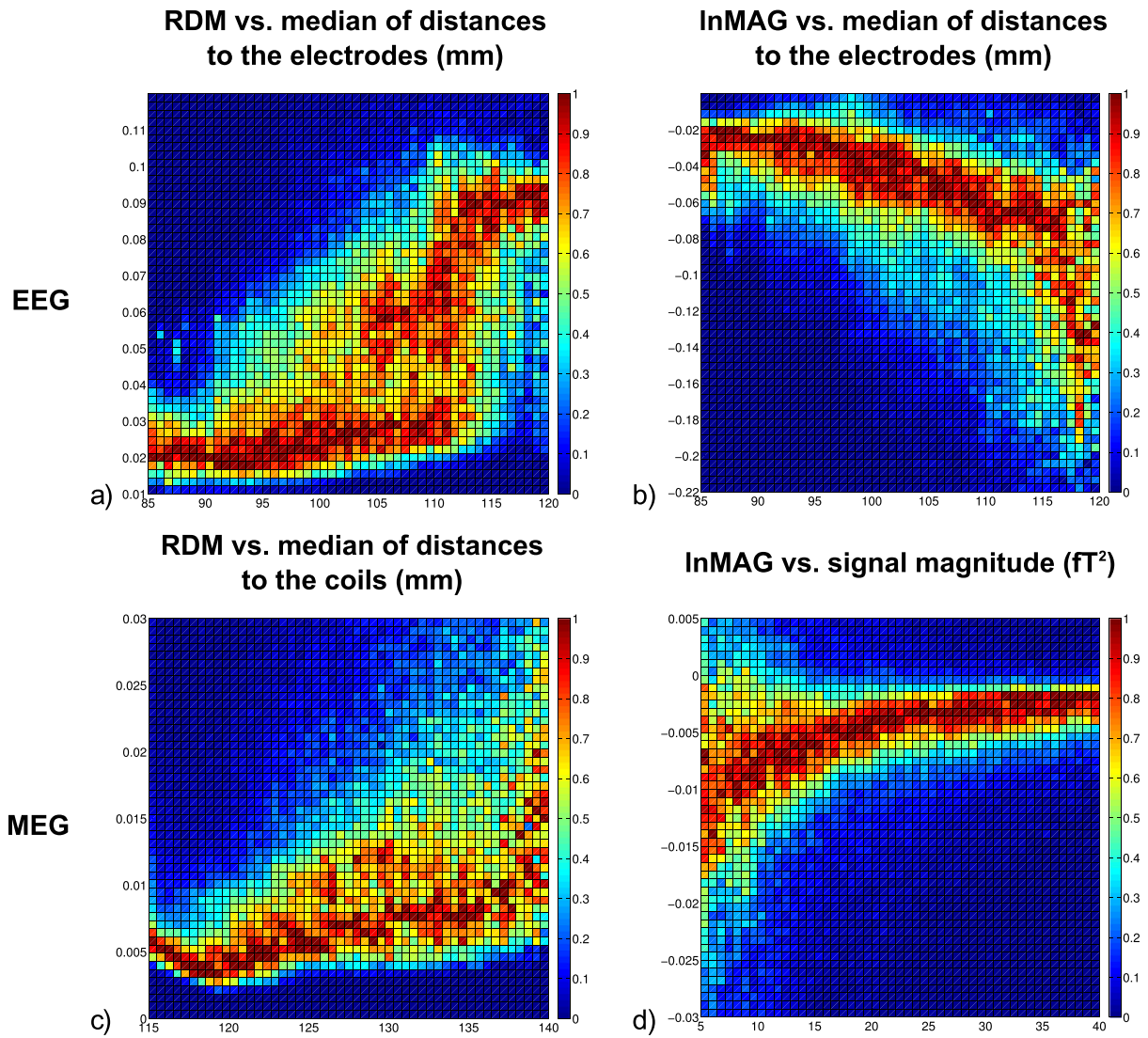
**RDM vs. median of distances to the electrodes (mm)**

**InMAG vs. median of distances to the electrodes (mm)**

**RDM vs. median of distances to the coils (mm)**

**InMAG vs. signal magnitude (fT²)**

EEG

MEG

**Fig. 13.** Effect of spongiosa/compacta distinction—difference between models *6CI* and *5CI* in 2D histogram.

Surely, these results do not imply that the skull plays a minor role in forward modeling. In contrast, much research was done with regard to skull modeling and it is now well known that the EEG is very sensitive to it, while the MEG is assumed to be mainly not affected as long as the inner skull surface is represented appropriately (Fuchs et al., 1998; Hämäläinen et al., 1993; Lew et al., 2013; Marin et al., 1998; van den Broek et al., 1998). However, Stenroos et al. (2014) have recently shown that assuming the skull to be fully insulating leads to errors that are larger than geometrical errors in a three-shell model and especially larger than those that are induced by assuming a homogeneous skull compartment. Skull conductivity parameters might vary across individuals and within the same individual due to variations in age, disease state, and environmental factors (Akhtari et al., 2002). The huge sensitivity of the EEG signal to these changes has been shown (Vallaghe and Clerc, 2009). The use of a suboptimal value for skull conductivity and skull conductivity uncertainties strongly influence the EEG as shown in various studies (Dannhauer et al., 2011; Fuchs et al., 1998; Huang et al., 2007; Lew et al., 2013; Montes-Restrepo et al., 2013). Recent studies have proposed ways to individually estimate parameters such as the skull conductivity (Aydin et al., 2014; Gonçalves et al., 2001, 2003; Huang et al., 2007; Wolters et al., 2010) that are important not only in EEG but also in combined EEG and MEG source analysis. It was furthermore shown that skull holes, included in

all of our models, play an important role for EEG, but are less important for MEG (Lanfer et al., 2012b; Lew et al., 2013; van den Broek et al., 1998). Ollikainen et al. (1999), Akhtari et al. (2002), Sadleir and Argibay (2007), and Dannhauer et al. (2011) studied the importance of skull inhomogeneity and of distinguishing skull compacta and spongiosa. However, Dannhauer et al. (2011) and Stenroos et al. (2014) have shown that differences between EEG and MEG forward solutions computed in models with skull spongiosa and compacta and those with homogenized isotropic skull can be kept at a rather small level compared to other effects by using an optimized isotropic skull conductivity parameter, as was done in this study. Our results are in line with the results of the MEG study by Stenroos et al. (2014), who found only small effects of neglecting the fine structure of the skull when using an optimized isotropic conductivity. The EEG study of Dannhauer et al. (2011) reported the strongest changes in motor areas, occipital and frontal lobe, while we found notable effects of skull spongiosa/compacta distinction for the EEG mainly in the temporal lobe as well as at the base of the frontal lobe and in some spots at the very top of the brain. Possible reasons for these differences might be found in the differing model setup. The head model used by Dannhauer et al. (2011) neglected the CSF compartment and thereby the here observed strong smearing effect was not present. This might have changed the influence of variations in the skull compartment to
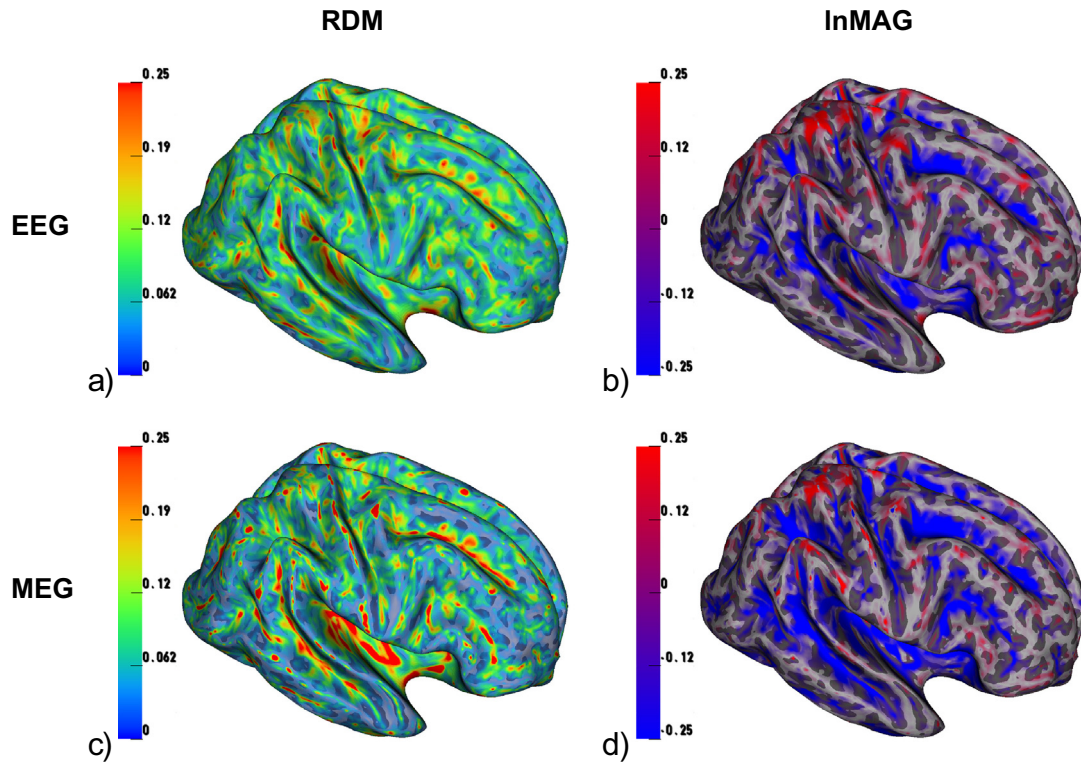
**RDM**                                              **lnMAG**



**Fig. 14.** Effect of white matter anisotropy—difference between models *6CA* and *6CI* plotted on brain surface.

the forward simulation. Furthermore, Dannhauer et al. (2011) used a conductivity of 0.0042 S/m for the isotropic skull compartment, while we already used their proposed optimized value of 0.01 S/m, which minimizes the differences between isotropic and multi compartment skull models.

The influence of modeling white matter anisotropy was also found to be strong, but less influential than that of CSF or brain compartment distinction (Figs. 4a and c, 5a and c), and the spatial distribution of the induced changes was difficult to interpret (Figs. 14, 15). We observed a decrease of signal magnitude with increasing source depth in both modalities (Figs. 15b and d), while the distribution of the topography effects was scattered with a trend towards higher effects for deeper sources (Figs. 14a and b, 15a and b).

Bangera et al. (2010) have experimentally shown that an anisotropic model leads to an improved performance when compared to isotropic models for the calculation of intracranial EEG forward solutions. Butson et al. (2007) and Chaturvedi et al. (2010) demonstrated in patient studies that the tissue activated by deep brain stimulation (DBS) can be reliably predicted by finite element simulations using realistic head models incorporating tissue anisotropy calculated following the approach of Tuch et al. (2001). These studies can be seen as an experimental validation of this approach also for EEG/MEG simulations, since the underlying mechanisms of volume conduction are identical. As further experimental evidence for the importance of modeling white matter anisotropy, Liehr and Haueisen (2008) presented phantom studies and demonstrated that anisotropic compartments influence directions, amplitudes, and shapes of potentials and fields at different degrees and conclude that anisotropic structures should be considered in volume conductor modeling when source orientation, strength, and extent are of interest.

Additionally, several simulation studies investigated the influence of white matter anisotropy on EEG and MEG source analysis. Haueisen et al. (2002) and Güllmar et al. (2010) investigated effects of white matter anisotropy on topography and magnitude measures in EEG and MEG source analysis. While these studies provide a comprehensive

evaluation of white matter anisotropy effects, our study adds a more detailed investigation of the spatial distribution of these effects and the comparison of effect strengths in relation to other important modeling effects. Even though Güllmar et al. (2010) visualized the effects for a fixed anisotropy of 1:10, the depicted effect distribution appears very similar to the one presented here. Their so-called *directv* approach showed the same tendency towards a negative lnMAG for both EEG and MEG when the cumulative relative frequency was plotted as it is visible in our Figs. 14 and 15. Of all their approaches it is the one that is most similar to the one used here, since it is also based on the model of Tuch et al. (2001). A more detailed comparison of the RDM effects is hardly possible, since the results were depicted as histograms by Güllmar et al. (2010) in contrast to the cumulative relative frequencies plotted here. For most sources they reported an RDM below 0.1, while we found slightly higher overall effects in our work. This might be explained by the different approaches used to scale the conductivity tensors. In the *directv* approach the tensors for each element are scaled so that they fit best to the isotropic conductivity. This results in a closer approximation to the isotropic model than our approach and thus leads to smaller relative effects. However, this does not allow for a conclusion which approach is more realistic, but only which is closer to the isotropic model. Haueisen et al. (2002) used the theoretically derived scaling factor from Tuch et al. (2001) to compute anisotropic conductivity tensors for both gray and white matter and also found a decrease of signal magnitude for deeper, dipolar sources in both EEG and MEG due to the introduction of anisotropic conductivity. The change in topography correlation between isotropic and anisotropic model was less clear. While the correlation in the MEG was still high and a—even though weak—depth dependency could be found, the EEG was more strongly affected, but the behavior was rather unsteady. Hallez et al. (2008) showed that particularly the omission of conductivity anisotropy leads to a large displacement of reconstructed sources that are oriented parallel to the fiber structure in the main direction of anisotropy, while it was considerably smaller for sources oriented perpendicular to the local fiber structure. Observed localization errors were up to 10 mm.
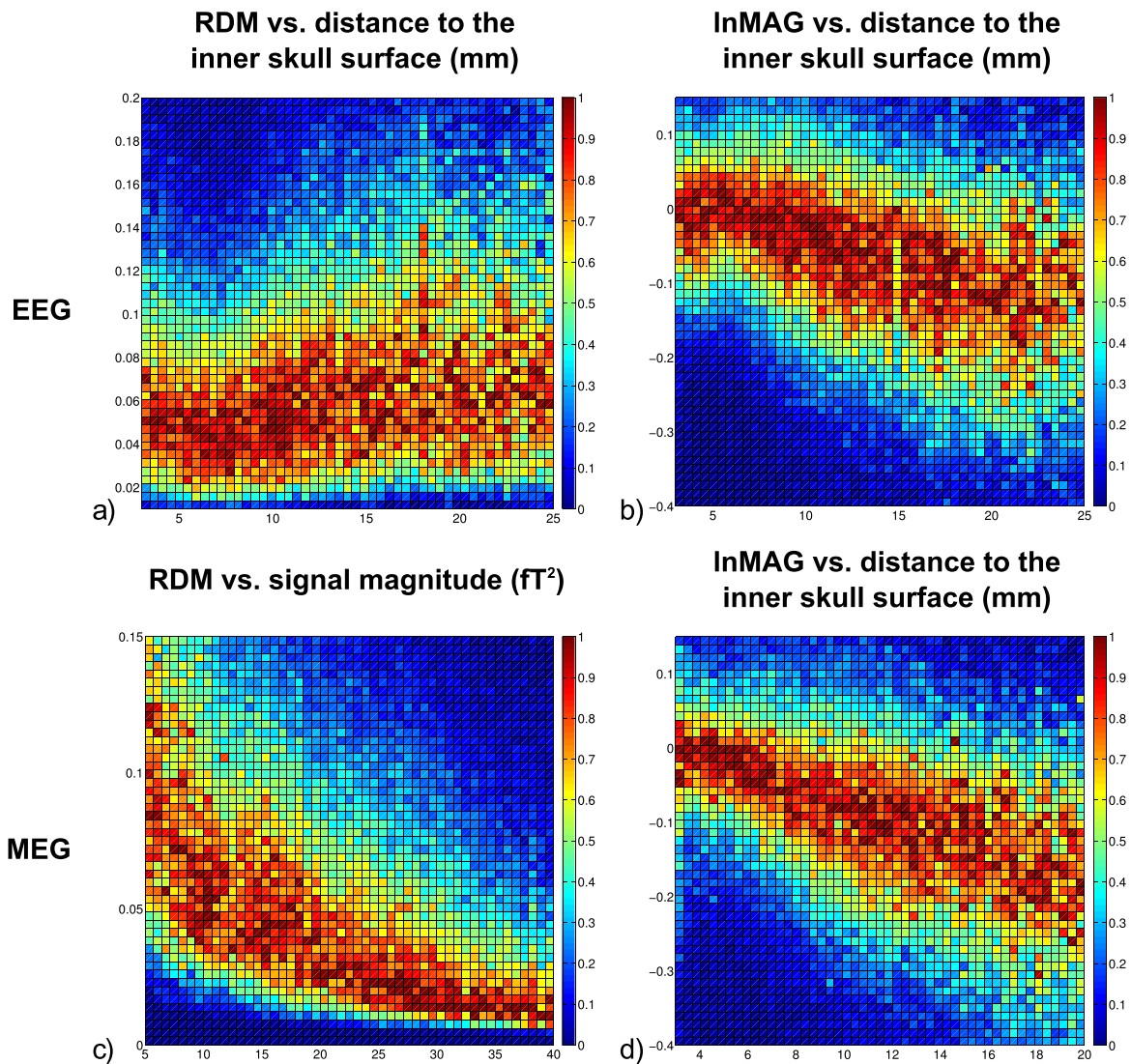
### RDM vs. distance to the inner skull surface (mm)

### lnMAG vs. distance to the inner skull surface (mm)

**EEG**

### RDM vs. signal magnitude (fT²)

### lnMAG vs. distance to the inner skull surface (mm)

**MEG**

**Fig. 15.** Effect of white matter anisotropy—difference between models *6CA* and *6CI* in 2D histogram.

Wolters et al. (2006) could show that white matter anisotropy causes volume currents to flow in directions more parallel to the white matter fiber tracts, with a clearly increased influence of white matter anisotropy on a deep source compared to superficial sources. However, they only investigated the effect of prolate anisotropy at fixed ratios on the forward solution for three sources; one deep in the thalamus and one radial and one tangential source in the somatosensory cortex.

In order to show the influence of changes in the forward solution on the inverse solution, Dannhauer et al. (2011) investigated the relationship between RDM and localization error for the EEG using scatter plots and correlation analysis. Although they did not find a unique relation, an undeniable correlation between these measures was observed. Upper and lower limits for the localization error were found to exist as linear functions of the RDM; a RDM of 0.025 predicted, for example, maximal localization errors between 8 and 10 mm and an RDM of 0.25 predicted minimal localization errors of about 2 mm. Therefore, even though our study focused on the forward problem, the conclusions derived for volume conductor modeling are directly related to the accuracy in the EEG and MEG inverse problem.

For the MEG on its own, the importance of the changing volume currents seems to be rather low, since the main results were changes in signal magnitude, while the topography was strongly affected only

for sources with a weak sensor signal. Indirectly, we were able to confirm the results of Ahlfors et al. (2010), who showed that—similar to spherical head models—also in the classic 3-compartment isotropic head model a source orientation to which the MEG is nearly insensitive exists. In our more realistic 6-compartment anisotropic head model scenario, we showed that the measured sensor signal in the MEG is still strongly influenced by source orientation and depth; namely, being weak for quasi-radial and deep sources, while the dependency of the EEG on these parameters is much weaker. This shows the benefits of EEG for source analysis in a variety of scenarios despite the stronger interference of volume conduction effects.

Nevertheless, all of these results, including those from this study, were gained under the assumption of point-like dipole sources. Since sources in practice might most often have an extent of at least some mm, not many purely quasi-radial sources at gyral crowns might exist in realistic scenarios. Hillebrand and Barnes (2002), e.g., conclude that source depth and not orientation is the main factor that compromises the sensitivity of MEG to activity in the adult human cortex. They argue that even if there are thin (approximately 2 mm wide) strips of poor MEG resolvability at the crests of gyri, these strips account for only a relatively small proportion of the cortical area and are abutted by elements with nominal tangential component and thus high resolvability due to their proximity to the sensor array. Our study clearly

showed that also in a 6-compartment anisotropic head model the strips of poor MEG resolvability are rather thin (see, e.g., Fig. 14). The presented effects for the weak quasi-radial sources at gyral crowns might therefore not be relevant in practice. But, when aiming to evaluate EEG and MEG data simultaneously, these effects become much more important in order to be able to explain the multimodal measurement.

A very important result of our study is that the comparison with the high resolution FE model showed the high numerical accuracy achieved with the FE approach. Several studies comparing the accuracy of different numerical approaches were carried out. As mentioned in the Materials and methods section, Lew et al. (2009) and Wolters et al. (2007) compared the accuracy of the different FE approaches—namely, the Venant, partial integration, and subtraction approach—using tetrahedral and hexahedral models, respectively. Both studies found that all of these approaches perform very well, with only small differences regarding accuracy, whereas the biggest differences were given regarding computation speed. Vorwerk et al. (2012) expanded on these comparisons by also evaluating numerical approaches using the boundary element method (BEM). Furthermore, in addition to sphere models, also realistically shaped 3-compartment head models (with compartments brain, skull and skin) were used as evaluation platform. Again, all numerical approaches achieved a good accuracy and the comparison to a realistically shaped 4-compartment head model including a CSF compartment already showed that the effect of model simplifications can be much larger than the accuracy differences between the examined numerical approaches. In this study, we demonstrated that not only the effect of CSF distinction, but also the effect of gray/white matter distinction or of modeling the white matter anisotropy, is clearly bigger than possible accuracy differences. Even the least influential modeling effect investigated in this study, the distinction of skull spongiosa/compacta, was still in the range of the numerical error between models 6CA and 6CA_hr. Thus, taking care to ensure the highly accurate generation of realistic head models to reduce the errors made by an insufficiently exact head modeling should not be forgotten over the development of new numerical approaches that might lead to a further improvement in—the already very good—numerical accuracy.

In order to achieve a high practical relevance of our results, we did not adjust the number of sensors between modalities. Instead, we used realistic sensor configurations as currently used in our lab, e.g., in epilepsy diagnosis (Aydin et al., 2014), since it can be assumed that these provide sufficient spatial sampling (Ahonen et al., 1993; Grieve et al., 2004; Lantz et al., 2003) so that the different number of sensors did not significantly influence our results. Additionally, we investigated the influence of sensor coverage on the observed effects. When investigating the effect of the distinction between skull spongiosa and skull compacta we found a relation between weak sensor coverage and an increased topography error, especially for the EEG. In practice, this issue can be addressed by using sensor caps reaching further downwards, thereby better covering the temporal lobe and the base of the frontal lobe.

#### Conclusion

We showed that a realistic modeling of the volume conductor has strong effects on both EEG and MEG that should be taken into account. Especially for superficial sources, which were often assumed to be less affected by volume conduction effects than deep sources, we found the strongest changes with regard to signal topography and magnitude. We conclude the following guideline for an accurate EEG/MEG forward simulation:

a) CSF: Our study systematically showed the importance of including the highly conductive CSF into the volume conductor for both EEG and MEG. This step only requires moderate additional effort in the segmentation procedure.

b) Gray/white matter distinction: The same conclusions as for the CSF hold true for the gray/white matter distinction. We found strong

effects for this modeling step, while the additional amount of work for including gray/white matter distinction into a volume conductor model is at a reasonable level.

c) White matter anisotropy: The inclusion of white matter anisotropy showed smaller (but still significant) effects than a) and b). However, the complexity of modeling anisotropy and the limitations of the underlying model have to be taken into account. Therefore, we would conclude that not modeling white matter anisotropy is admissible until the last doubts in a realistic modeling of white matter anisotropy (sufficient DTI resolution, appropriate scaling between diffusion and conductivity tensors) have been eliminated.

d) Skull: The distinction between skull compacta and spongiosa showed weak effects especially for the MEG. Thus, it might in most cases be disregarded for the MEG. For the EEG, distinguishing different skull compartments is clearly less important than the previously mentioned modeling steps, especially when using an optimized conductivity value for the homogenized skull. However, the otherwise high importance of an accurate modeling of the skull was shown in a variety of studies and was therefore not the focus of this study. The influence of the uncertainty in the skull conductivity values found in the literature should not be underestimated and a conductivity calibration should be considered.

In summary, this study shows the most reasonable steps one should take to expand the commonly used 3-layer head model by additional compartments. Furthermore, this study demonstrates that the numerical inaccuracies of the finite element approach used appear negligible compared to these modeling effects.

#### References

Ahlfors, S.P., Han, J., Belliveau, J.W., Hämäläinen, M., 2010. Sensitivity of MEG and EEG to source orientation. Brain Topogr. 23 (3), 227–232. http://dx.doi.org/10.1007/s10548-010-0154-x.

Ahonen, A.I., Hämäläinen, M., Ilmoniemi, R.J., Kajola, M.J., Knuutila, J., Simola, J.T., Vilkman, V.V., 1993. Sampling theory for neuromagnetic detector arrays. IEEE Trans. Biomed. Eng. 40 (9), 859–869. http://dx.doi.org/10.1109/10.245606.

Akhtari, M., Bryant, H.C., Mamelak, A.N., Flynn, E.R., Heller, L., Shih, J.J., Mandelkern, M., et al., 2002. Conductivities of three-layer live human skull. Brain Topogr. 14 (3), 151–167. http://dx.doi.org/10.1023/A:1014590923185.

Astolfi, L., Cincotti, F., Mattia, D., Babiloni, C., Carducci, F., Basilisco, A., Rossini, P.M., et al., 2005. Assessing cortical functional connectivity by linear inverse estimation and directed transfer function: simulations and application to real data. Clin. Neurophysiol. 116 (4), 920–932. http://dx.doi.org/10.1016/j.clinph.2004.10.012.

Aydin, Ü., Vorwerk, J., Küpper, P., Heers, M., Kugel, H., Galka, A., Hamid, L., et al., 2014. Combining EEG and MEG for the reconstruction of epileptic activity using a calibrated realistic volume conductor model. PLoS ONE 9 (3), e93154. http://dx.doi.org/10.1371/journal.pone.0093154.

Bangera, N.B., Schomer, D.L., Dehghani, N., Ulbert, I., Cash, S., Papavasiliou, S., Eisenberg, S.R., Dale, A.M., Halgren, E., 2010. Experimental validation of the influence of white matter anisotropy on the intracranial EEG forward solution. J. Comput. Neurosci. 29 (3), 371–387. http://dx.doi.org/10.1007/s10827-009-0205-z.

Baumann, S.B., Wozny, D.R., Kelly, S.K., Meno, F.M., 1997. The electrical conductivity of human cerebrospinal fluid at body temperature. IEEE Trans. Biomed. Eng. 44 (3), 220–223. http://dx.doi.org/10.1109/10.554770.

Bijsterbosch, J.D., Lee, K.-H., Hunter, M.D., Wilkinson, I.D., Farrow, T., Barker, A.T., Woodruff, P.W.R., 2013. The effect of head orientation on subarachnoid cerebrospinal fluid distribution and its implications for neurophysiological modulation and recording techniques. Physiol. Meas. 34 (3), N9. http://dx.doi.org/10.1088/0967-3334/34/3/N9.

Brette, R., Destexhe, A., 2012. Handbook of Neural Activity Measurement. Cambridge University Press.

Buchner, H., Knoll, G., Fuchs, M., Rienäcker, A., Beckmann, R., Wagner, M., Silny, J., Pesch, J., 1997. Inverse localization of electric dipole current sources in finite element models of the human head. Electroencephalogr. Clin. Neurophysiol. 102 (4), 267–278. http://dx.doi.org/10.1016/S0013-4694(96)95698-9.

Butson, C.R., Cooper, S.E., Henderson, J.M., McIntyre, C.C., 2007. Patient-specific analysis of the volume of tissue activated during deep brain stimulation. NeuroImage 34 (2), 661–670. http://dx.doi.org/10.1016/j.neuroimage.2006.09.034.

Chaturvedi, A., Butson, C.R., Lempka, S.F., Cooper, S.E., McIntyre, C.C., 2010. Patient-specific models of field model complexity on neural activation predictions. Brain Stimulation 3 (2), 65–77. http://dx.doi.org/10.1016/j.brs.2010.01.003.

Dannhauer, M., Lanfer, B., Wolters, C.H., Knösche, T.R., 2011. Modeling of the human skull in EEG source analysis. Hum. Brain Mapp. 32 (9), 1383–1399. http://dx.doi.org/10.1002/hbm.21114.

Dassios, G., Fokas, A.S., Hadjiloizi, D., 2007. On the complementarity of electroencephalography and magnetoencephalography. Inverse Probl. 23 (6), 2541. http://dx.doi.org/10.1088/0266-5611/23/6/016.

De Munck, J.C., Peters, M.J., 1993. A fast method to compute the potential in the multisphere model (EEG application). IEEE Trans. Biomed. Eng. 40 (11), 1166–1174. http://dx.doi.org/10.1109/10.245635.

Drechsler, F., Wolters, C.H., Dierkes, T., Si, H., Grasedyck, L., 2009. A full subtraction approach for finite element method based source analysis using constrained Delaunay tetrahedralisation. NeuroImage 46 (4), 1055–1065. http://dx.doi.org/10.1016/j.neuroimage.2009.02.024.

Fuchs, M., Wagner, M., Wischmann, H.-A., Köhler, T., Theißen, A., Drenckhahn, R., Buchner, H., 1998. Improving source reconstructions by combining bioelectric and biomagnetic data. Electroencephalogr. Clin. Neurophysiol. 107 (2), 93–111. http://dx.doi.org/10.1016/S0013-4694(98)00046-7.

Goldenholz, D.M., Ahlfors, S.P., Hämäläinen, M., Sharon, D., Ishitobi, M., Vaina, L.M., Stufflebeam, S.M., 2009. Mapping the signal-to-noise-ratios of cortical sources in magnetoencephalography and electroencephalography. Hum. Brain Mapp. 30 (4), 1077–1086. http://dx.doi.org/10.1002/hbm.20571.

Gonçalves, S.I., de Munck, J.C., Verbunt, J.P.A., 2001. In vivo measurement of skull and brain resistivities with EIT based method and analysis of SEF/SEP data. Proceedings of the 23rd Annual International Conference of the IEEE Engineering in Medicine and Biology Society, 2001, vol.1, pp. 1006–1008. http://dx.doi.org/10.1109/IEMBS.2001.1019124.

Gonçalves, S.I., de Munck, J.C., Verbunt, J.P.A., Bijma, F., Heethaar, R.M., Lopes da Silva, F., 2003. In vivo measurement of the brain and skull resistivities using an EIT-based method and realistic models for the head. IEEE Trans. Biomed. Eng. 50 (6), 754–767.

Grieve, P.G., Emerson, R.G., Isler, J.R., Stark, R.I., 2004. Quantitative analysis of spatial sampling error in the infant and adult electroencephalogram. NeuroImage 21 (4), 1260–1274. http://dx.doi.org/10.1016/j.neuroimage.2003.11.028.

Güllmar, D., Haueisen, J., Reichenbach, J.R., 2010. Influence of anisotropic electrical conductivity in white matter tissue on the EEG/MEG forward and inverse solution. A High-Resolution Whole Head Simulation Study. NeuroImage 51 (1), 145–163. http://dx.doi.org/10.1016/j.neuroimage.2010.02.014.

Hallez, H., Vanrumste, B., Van Hese, P., Delputte, S., Lemahieu, I., 2008. Dipole estimation errors due to differences in modeling anisotropic conductivities in realistic head models for EEG source analysis. Phys. Med. Biol. 53 (7), 1877. http://dx.doi.org/10.1088/0031-9155/53/7/005.

Hämäläinen, M., Hari, R., Ilmoniemi, R.J., Knuutila, J., Lounasmaa, O.V., 1993. Magnetoencephalography—theory, instrumentation, and applications to noninvasive studies of the working human brain. Rev. Mod. Phys. 65 (2), 413–497. http://dx.doi.org/10.1103/RevModPhys.65.413.

Haueisen, J., Ramon, C., Eiselt, M., Brauer, H., Nowak, H., 1997. Influence of tissue resistivities on neuromagnetic fields and electric potentials studied with a finite element model of the head. IEEE Trans. Biomed. Eng. 44 (8), 727–735. http://dx.doi.org/10.1109/10.605429.

Haueisen, J., Ramon, C., Brauer, H., Nowak, H., 2000. The influence of local tissue conductivity changes on the magnetoencephalogram and the electroencephalogram. Biomed. Tech. Biomed. Eng. 45 (7–8), 211–214.

Haueisen, J., Tuch, D.S., Ramon, C., Schimpf, P.H., Wedeen, V.J., George, J.S., Belliveau, J.W., 2002. The influence of brain tissue anisotropy on human EEG and MEG. NeuroImage 15 (1), 159–166. http://dx.doi.org/10.1006/nimg.2001.0962.

Heidemann, R.M., Porter, D.A., Anwander, A., Feiweier, T., Heberlein, K., Knösche, T.R., Turner, R., 2010. Diffusion imaging in humans at 7 T using readout-segmented EPI and GRAPPA. Magn. Reson. Med. 64 (1), 9–14. http://dx.doi.org/10.1002/mrm.22480.

Hillebrand, A., Barnes, G.R., 2002. A quantitative assessment of the sensitivity of whole-head MEG to activity in the adult human cortex. NeuroImage 16 (3, Part A), 638–650. http://dx.doi.org/10.1006/nimg.2002.1102.

Huang, M.-X., Song, T., Hagler Jr., D.J., Podgorny, I., Jousmaki, V., Cui, L., Gaa, K., et al., 2007. A novel integrated MEG and EEG analysis method for dipolar sources. NeuroImage 37 (3), 731–748. http://dx.doi.org/10.1016/j.neuroimage.2007.06.002.

Iwasaki, M., Pestana, E., Burgess, R.C., Lüders, H.O., Shamoto, H., Nakasato, N., 2005. Detection of epileptiform activity by human interpreters: blinded comparison between electroencephalography and magnetoencephalography. Epilepsia 46 (1), 59–68. http://dx.doi.org/10.1111/j.0013-9580.2005.21104.x.

Lanfer, B., Paul-Jordanov, I., Scherg, M., Wolters, C.H., 2012a. Influence of interior cerebrospinal fluid compartments on EEG source analysis. Biomed. Tech. Biomed. Eng. http://dx.doi.org/10.1515/bmt-2012-4020 (August).

Lanfer, B., Scherg, M., Dannhauer, M., Knösche, T.R., Burger, M., Wolters, C.H., 2012b. Influences of skull segmentation inaccuracies on EEG source analysis. NeuroImage 62 (1), 418–431. http://dx.doi.org/10.1016/j.neuroimage.2012.05.006.

Lantz, G., Grave de Peralta, R., Spinelli, L., Seeck, M., Michel, C.M., 2003. Epileptic source localization with high density EEG: how many electrodes are needed? Clin. Neurophysiol. 114 (1), 63–69.

Lew, S., Wolters, C.H., Dierkes, T., Röer, C., MacLeod, R.S., 2009. Accuracy and run-time comparison for different potential approaches and iterative solvers in finite element method based EEG source analysis. Appl. Numer. Math. 59 (8), 1970–1988. http://dx.doi.org/10.1016/j.apnum.2009.02.006.

Lew, S., Sliva, D.D., Choe, M.-S., Grant, P.E., Okada, Y., Wolters, C.H., Hämäläinen, M., 2013. Effects of sutures and fontanels on MEG and EEG source analysis in a realistic infant head model. NeuroImage 76 (August), 282–293. http://dx.doi.org/10.1016/j.neuroimage.2013.03.017.

Liehr, M., Haueisen, J., 2008. Influence of anisotropic compartments on magnetic field and electric potential distributions generated by artificial current dipoles inside a torso phantom. Phys. Med. Biol. 53 (1), 245. http://dx.doi.org/10.1088/0031-9155/53/1/017.

Lin, F.-H., Hara, K., Solo, V., Vangel, M., Belliveau, J.W., Stufflebeam, S.M., Hämäläinen, M., 2009. Dynamic Granger–Geweke causality modeling with application to interictal spike propagation. Hum. Brain Mapp. 30 (6), 1877–1886. http://dx.doi.org/10.1002/hbm.20772.

Marin, G., Guerin, C., Baillet, S., Garnero, L., Meunier, G., 1998. Influence of skull anisotropy for the forward and inverse problem in EEG: simulation studies using FEM on realistic head models. Hum. Brain Mapp. 6 (4), 250–269. http://dx.doi.org/10.1002/(SICI)1097-0193(1998)6:4<250::AID-HBM5>3.0.CO;2-2.

Meijs, J.W.H., Weier, O.W., Peters, M.J., Van Oosterom, A., 1989. On the numerical accuracy of the boundary element method (EEG application). IEEE Trans. Biomed. Eng. 36 (10), 1038–1049. http://dx.doi.org/10.1109/10.40805.

Montes-Restrepo, V., van Mierlo, P., Strobbe, G., Staelens, S., Vandenberghe, S., Hallez, H., 2013. Influence of skull modeling approaches on EEG source localization. Brain Topogr. http://dx.doi.org/10.1007/s10548-013-0313-y (September).

Oh, S.H., Lee, S.Y., Cho, M.H., Kim, T.S., Kim, I.H., 2006. Electrical conductivity estimation from diffusion tensor and T2: A Silk Yarn Phantom Study. Proc Intl Soc Mag Reson Med, 14, p. 3034 (http://afni.nimh.nih.gov/sscc/staff/rwcox/ISMRM_2006/ISMRM%202006%20-%203340/files/03034.pdf).

Ollikainen, J.O., Vauhkonen, M., Karjalainen, P.A., Kaipio, J.P., 1999. Effects of local skull inhomogeneities on EEG source estimation. Med. Eng. Phys. 21 (3), 143–154. http://dx.doi.org/10.1016/S1350-4533(99)00038-7.

Oostenveld, R., Oostendorp, T.F., 2002. Validating the boundary element method for forward and inverse EEG computations in the presence of a hole in the skull. Hum. Brain Mapp. 17 (3), 179–192. http://dx.doi.org/10.1002/hbm.10061.

Pohlmeier, R., Buchner, H., Knoll, G., Rienäcker, A., Beckmann, R., Pesch, J., 1997. The influence of skull-conductivity misspecification on inverse source localization in realistically shaped finite element head models. Brain Topogr. 9 (3), 157–162. http://dx.doi.org/10.1007/BF01190384.

Ramon, C., Schimpf, P., Haueisen, J., Holmes, M., Ishimaru, A., 2004. Role of soft bone, CSF and gray matter in EEG simulations. Brain Topogr. 16 (4), 245–248. http://dx.doi.org/10.1023/B:BRAT.0000032859.68959.76.

Rice, J.K., Rorden, C., Little, J.S., Parra, L.C., 2013. Subject position affects EEG magnitudes. NeuroImage 64 (January), 476–484. http://dx.doi.org/10.1016/j.neuroimage.2012.09.041.

Rullmann, M., Anwander, A., Dannhauer, M., Warfield, S.K., Duffy, F.H., Wolters, C.H., 2009. EEG source analysis of epileptiform activity using a 1 Mm anisotropic hexahedra finite element head model. NeuroImage 44 (2), 399–410. http://dx.doi.org/10.1016/j.neuroimage.2008.09.009.

Ruthotto, L., Kugel, H., Olesch, J., Fischer, B., Modersitzki, J., Burger, M., Wolters, C.H., 2012. Diffeomorphic susceptibility artifact correction of diffusion-weighted magnetic resonance images. Phys. Med. Biol. 57 (18), 5715. http://dx.doi.org/10.1088/0031-9155/57/18/5715.

Sadleir, R.J., Argibay, A., 2007. Modeling skull electrical properties. Ann. Biomed. Eng. 35 (10), 1699–1712. http://dx.doi.org/10.1007/s10439-007-9343-5.

Salayev, K.A., Nakasato, N., Ishitobi, M., Shamoto, H., Kanno, A., Iinuma, K., 2006. Spike orientation may predict epileptogenic side across cerebral sulci containing the estimated equivalent dipole. Clin. Neurophysiol. 117 (8), 1836–1843. http://dx.doi.org/10.1016/j.clinph.2006.05.003.

Schimpf, P.H., Ramon, C., Haueisen, J., 2002. Dipole models for the EEG and MEG. IEEE Trans. Biomed. Eng. 49 (5), 409–418. http://dx.doi.org/10.1109/10.995679.

Stenroos, M., Hunold, A., Haueisen, J., 2014. Comparison of three-shell and simplified volume conductor models in magnetoencephalography. NeuroImage 94 (5), 337–348.

Taubin, G., 1995. A signal processing approach to fair surface design. Proceedings of the 22nd Annual Conference on Computer Graphics and Interactive Techniques. ACM, New York, NY, USA, pp. 351–358. http://dx.doi.org/10.1145/218380.218473 (SIGGRAPH '95).

Tuch, D.S., van Wedeen, J., Dale, A.M., George, J.S., Belliveau, J.W., 2001. Conductivity tensor mapping of the human brain using diffusion tensor MRI. Proc. Natl. Acad. Sci. 98 (20), 11697–11701. http://dx.doi.org/10.1073/pnas.171473898.

Vallaghe, S., Clerc, M., 2009. A global sensitivity analysis of three- and four-layer EEG conductivity models. IEEE Trans. Biomed. Eng. 56 (4), 988–995. http://dx.doi.org/10.1109/TBME.2008.2009315.

Van den Broek, S.P., Reinders, F., Donderwinkel, M., Peters, M.J., 1998. Volume conduction effects in EEG and MEG. Electroencephalogr. Clin. Neurophysiol. 106 (6), 522–534. http://dx.doi.org/10.1016/S0013-4694(97)00147-8.

Van Uitert, R., Johnson, C., Zhukov, L., 2004. Influence of head tissue conductivity in forward and inverse magnetoencephalographic simulations using realistic head models. IEEE Trans. Biomed. Eng. 51 (12), 2129–2137. http://dx.doi.org/10.1109/TBME.2004.836490.

Vese, L.A., Chan, T.F., 2002. A multiphase level set framework for image segmentation using the Mumford and Shah model. Int. J. Comput. Vis. 50 (3), 271–293. http://dx.doi.org/10.1023/A:1020874308076.

Vorwerk, J., 2011. Comparison of Numerical Approaches to the EEG Forward Problem. http://wwwmath.uni-muenster.de/num/Arbeitsgruppen/ag_burger/organization/burger/pictures/DA%20Vorwerk.pdf.

Vorwerk, J., Clerc, M., Burger, M., Wolters, C.H., 2012. Comparison of boundary element and finite element approaches to the EEG forward problem. Biomed. Tech. Biomed. Eng. 57 (August). http://dx.doi.org/10.1515/bmt-2012-4152.

Wendel, K., Narra, N.G., Hannula, M., Kauppinen, P., Malmivuo, J., 2008. The influence of CSF on EEG sensitivity distributions of multilayered head models. IEEE Trans. Biomed. Eng. 55 (4), 1454–1456. http://dx.doi.org/10.1109/TBME.2007.912427.

Wolters, C.H., Grasedyck, L., Hackbusch, W., 2004. Efficient computation of lead field bases and influence matrix for the FEM-Based EEG and MEG inverse problem. Inverse Probl. 20 (4), 1099. http://dx.doi.org/10.1088/0266-5611/20/4/007.

Wolters, C.H., Anwander, A., Tricoche, X., Weinstein, D., Koch, M.A., MacLeod, R.S., 2006. Influence of tissue conductivity anisotropy on EEG/MEG field and return current computation in a realistic head model: a simulation and visualization study using high-resolution finite element modeling. NeuroImage 30 (3), 813–826. http://dx.doi.org/10.1016/j.neuroimage.2005.10.014.

Wolters, C.H., Köstler, H., Möller, C., Härdtlein, J., Anwander, A., 2007. Numerical approaches for dipole modeling in finite element method based source analysis. Int. Congr. Ser. 1300 (June), 189–192. http://dx.doi.org/10.1016/j.ics.2007.02.014.

Wolters, C.H., Lew, S., MacLeod, R.S., Hämäläinen, M., 2010. Combined EEG/MEG Source Analysis Using Calibrated Finite Elementhead Models. Proceedings of the 4th Annual Conference of the German Society for Biomedical Engineering (DGBMT'10) (http://www.sci.utah.edu/~wolters/PaperWolters/WoltersEtAl_BMT_2010.pdf).